MID-COURSE GUIDANCE SIMULATION FOR ANTI-AIR MISSILE SYSTEMS

By

EDWIN JAMES WALLER

Bachelor of Science
Oklahoma State University
Stillwater, Oklahoma
1949

Master of Science
Oklahoma State University
Stillwater, Oklahoma
1951

Engineer
Stanford University
Stanford, California
1959

Submitted to the Faculty of the
Graduate College of the
Oklahoma State University
in partial fulfillment of
the requirements for
the Degree of
DOCTOR OF PHILOSOPHY
May, 1968

MID-COURSE GUIDANCE SIMULATION FOR ANTI-AIR MISSILE SYSTEMS

Thesis Approved:

J. K. Norton
Thesis Adviser

Harold Smith

Paul A. McCollum

G. B. Thurston

N. Durham
Dean of the Graduate College

PREFACE

This thesis was intended to extend the knowledge of mid-course guidance, particularly so terminal guidance inputs could be predicted more reliably.

A study of the mid-course guidance of anti-air missiles using proportional navigation was carried out. This guidance, which commences after launch and continues to some point near the target when terminal guidance begins, was expressed mathematically in three dimensions. The missile-target encounter was simulated using an analog computer in which various heading and position errors and target maneuvers were purposely programmed.

The analog computer, a TR-48 (EAI), does not contain enough amplifiers and multipliers to simulate the complete system of nonlinear equations. However, an approximation of the system allows reduction in complexity, and, thereby, fewer multipliers and amplifiers are needed.

I would like to express my appreciation to the following:

To Professor J. R. Norton, my committee chairman, for his encouragement and help throughout my career;

To the other members of my committee,

Professor H. T. Fristoe, Professor P. A. McCollum, and Professor G. B. Thurston, for their contributions;

To my wife for her editorial ability and her understanding during a difficult period;

To the National Science Foundation for its financial assistance;

To Mr. Frank McClesky of the Naval Weapons Laboratory in Dahlgren, Virginia;

To the School of Mechanical Engineering for use of the analog computer;

To the United States Naval Academy, Captain A. H. McCain, and my associates in the Weapons Department; and

To Velda Davis for her typing of this thesis.

TABLE OF CONTENTS

Chapter		Page
I.	INTRODUCTION	1
	Missile Systems	2
	Mid-Course Guidance	4
	Proportional Guidance	8
II.	SIGNIFICANT HISTORICAL CONTRIBUTIONS	12
	Guided Missiles and Rockets	12
	Mid-Course Guidance	17
III.	KINEMATIC ANALYSIS OF MISSILE AND TARGET ENCOUNTER	20
	Reference Systems	20
	Range and Range Rate Equations	22
	Missile Velocity	27
	Proportional Navigation	29
	Missile Transfer Function	30
	Nonlinear System	31
	Linearization of Equations	32
	Nonlinear Approximate Equations	36
IV.	ANALOG COMPUTER SIMULATION	38
	Unscaled System	38
	Encounter Conditions	41
	Estimated Maximum of Variables for Error Encounters	43
	Scaled Computer Diagrams	44
	Target Maneuver	49
V.	ANALOG COMPUTER RESULTS	54
	Introduction	54
	Calibration	54
	Missile and Target Heading and Position Errors	56
	Target Maneuver	59
	General Results	60

Chapter Page

VI. SUMMARY AND CONCLUSIONS 89

Summary 89
Conclusions 91
Recommended Future Studies 93

BIBLIOGRAPHY 95

APPENDIX A 97

APPENDIX B 101

LIST OF TABLES

Table		Page
I.	Collision Course Data	43
II.	Amplitude Scaling - Error Encounters	45
III.	Amplitude Scaling - Target Maneuver	51
IV.	Initial Position and Heading Errors	62
V.	Target Maneuver Encounter Conditions	66
VI.	Calibration Results	85
VII.	Position and Heading Error Results	86
VIII.	Target Maneuver Results	88

LIST OF FIGURES

Figure		Page
1.	Typical Missile Flight Paths	5
2.	Collision Course	9
3.	Coordinate System for Two-Dimensional Homing Interception	9
4.	Missile and Target Geometry	21
5.	Coordinate Systems and Axes	21
6.	Range Vector, $\overline{R}$	25
7.	Missile Velocity, $\overline{V}_M$	25
8.	Scaled Computer Diagram - Error Encounter	46
9.	Scaled Computer Diagram - Error Encounter (Continued)	47
10.	Scaled Computer Diagram - Error Encounter (Continued)	48
11.	Scaled Computer Diagram - Maneuver Generator	52
12.	Calibration of Simulation System	67
13.	Calibration	68
14.	Encounter III, Run 11	70
15.	Encounter IV, Run 3	74
16.	Encounter V, Runs 4 and 5	76
17.	Encounter VI, Run 2b	77
18.	Encounter VI, Run 2e	78
19.	Encounter VI, Run 2c	79
20.	Encounter VI, Run 2d	80

Figure Page

21. Encounter VI, Run 3c 81

22. Encounter VI, Run 3d 82

23. Encounter VI, Run 4c 83

24. Encounter VI, Run 5a 84

25. Coordinate Systems 97

LIST OF SYMBOLS

A	The angle from the line of sight to the target velocity vector; clockwise is positive.
G	Transfer function for the missile, either yaw or pitch mode.
i	Unit vector along the collision course missile path, x_M.
I	Unit vector along the initial range vector, R_o.
j	Unit vector along y_M axis.
J	Unit vector along y_1 axis in the initial collision course plane.
k	Unit vector along z_1 and z_M axes which are perpendicular to the collision course plane.
L	Lead angle, the angle from the line of sight to the missile velocity vector; clockwise is positive.
M	The missile position; with bar, means the vector; with subscript, refers to specific time.
N	Navigation ratio.
R	The range from the missile to the target; with a bar, means the vector; with a subscript, refers to a specific time or axis; see subscript note.

s	The Laplace subsidiary variable.
T	The target position; with bar, means the vector; with subscript, refers to specific time.
u, $\dot{u}$	The perturbations of position and velocity coordinates along the target collision course measured from the collision course solution.
u_t, $\dot{u}_t$	The position and velocity of the target measured from the initial target references T_o along the collision course.
u_t, v_t, w_t	The target reference axes.
u, v, w	The perturbations of the target reference axes.
V	Speed; i.e., the magnitude of a velocity vector; see subscripts for specific term.
$\overline{V}$	Velocity vector; see subscripts for specific term.
x, y, z	The perturbation of the missile reference axes.
x_1, y_1, z_1	The line of sight reference axes.
x_M, y_M, z_M	The missile reference axes.
α_x, α_y, α_z	Direction angles for the x_1, y_1, and z_1 axes.
γ	The change in lead angle measured from the collision course in the collision course plane.
Γ_{Mo}	The direction angle for the missile velocity $\overline{V}_{Mo}$.
Γ_{to}	The direction angle for the target velocity $\overline{V}_{to}$.

δ, φ_R	The change in the line of sight angle measured in a plane perpendicular to the collision course plane.
ε_1 , ε_2	Unit vectors along the u_t and v_t axes.
θ_M	The angle with x_1 , y_1 plane locating the missile velocity vector (Figure 7).
θ_R, λ	The change in the line of sight angle measured in the collision plane.
λ, θ_R	The change in the line of sight angle measured in the collision plane.
Λ	The direction angle for the initial line of sight in the collision course plane.
ρ_M	The missile position coordinate; with a bar, means the vector; with a subscript refers to the scalar component along one of the x_1 , y_1 , z_1 axes. A dot above signifies one derivative with time.
ρ_t	The target position coordinate; with a bar, means the vector; with a subscript refers to the scalar component along one of the x_1 , y_1 , z_1 axes. A dot above signifies one derivative with time.
σ, φ_M	The change in the direction of the missile velocity measured from the collision course plane.
φ_M , σ	The change in the direction of the missile

velocity measured from the collision course plane.

φ_R, δ — The change in the line of sight direction measured from the collision course plane.

Symbols used as subscripts

M — Refers to missile at any time.

M_o — Refers to missile at the initiation of mid-course guidance.

t — Refers to target at any time.

tO — Refers to target at the initiation of mid-course guidance.

O — Refers to the variable at the initiation of mid-course guidance.

1 — Refers to the collision course solution at some time t.

p — Refers to the perturbed solution at the same time t_1 above.

x, y, z — Denotes the scalar component of the variable along the initial line of sight reference frame (x_1, y_1, z_1).

CHAPTER I

INTRODUCTION

The objective of the research described in this thesis was to develop a technique for simulation of mid-course guidance of anti-air missile systems capable of being extended to real systems when actual missile and target dynamics are used. The simulation was designed to yield the miss-distance and missile to target attitude angles for initial missile heading errors and for target maneuver. Proportional navigation was selected as the guidance scheme. The primary goal was to extend the present two-dimensional concepts to three-dimensional target maneuver.

Although not required of this research, it appears appropriate to indicate possible uses of this work. The research provides a basis for determination of statistical values of miss-distance and attitude for the design evaluation of new missile systems.

The system inputs are as follows:

(1) heading errors;

(2) sensor noise;

(3) target maneuver; and

(4) launch delay.

Missile Systems

The missile undergoes five general phases of operation. These are:

(1) storage and pre-launch;

(2) launching;

(3) propulsion;

(4) glide to intercept; and

(5) target intercept (i.e., terminal).

The reliability of each of these phases is the prime consideration, both in missile system design and in tactical use of the system.

The design evaluation of the missile culminates in a single shot kill probability which depends on the product of the probabilities of individual sub-system operation. One of the most important factors in the evaluation is at intercept, where the missile has been guided by some means. Starting at some relative position (distance and angle), the fuse acquires the target; at some subsequent position, explodes the warhead, and, ideally, the kill mechanism strikes a vulnerable part of the target. The terminal analysis is statistically oriented, drawing generously on gaming theory. The main inputs to the analysis are the vector quantities of relative displacement (range and attitude) and relative velocity (range rate). These quantities are the outputs of the guidance from launch to intercept.

Guidance

There are many different schemes for guidance of missiles. However, most systems are characterized in the following manner:

(1) pre-set at launch;

(2) updating after the launch;

(3) mid-course guidance; and

(4) terminal guidance.

The first two are best illustrated by examples. In air-to-air missiles (A.A.M.), the aircraft aims the missile by aiming itself. In certain cases, a downward component is given so that the missile clears the launch vehicle. Shortly thereafter, the launch computer system updates the course and commands the missile on to a corrected intercept course. For surface to air (S.A.M.), a launcher is pre-set with updating in flight shortly after launch.

Mid-course guidance occurs when the missile is in flight to the target. The missile has been commanded to fly an intercept path to the target. If the missile and target position and velocities are actually as predicted by the sensors and computers, and if no changes occur in flight, then the missile should intercept the target with a direct hit. This generally is not the case, and guidance is necessary.

Terminal guidance is generally linked with the fusing mechanism which explodes the warhead so that maximum kill is achieved.

This research is concerned primarily with mid-course guidance, of which there are four general types. These are called "Preset Variable Guided Flight Paths," and are shown in Figure 1 (1, p. 181).

Mid-Course Guidance

The four general types of mid-course guidance (as shown in Figure 1) are: pursuit, beam riding, constant bearing or command course, and proportional navigation. The salient features of each are:

(1) Pursuit Courses. The pure pursuit course is defined as that described by a missile which always heads directly toward the target. The most important parameter is the missile-to-target velocity ratio, which must be greater than one and less than two, in the ideal case. Values greater than two require infinite missile acceleration as the missile approaches the target, while values less than one require infinite time of flight. In general, for a missile with a given upper limit of acceleration, there is a region of permissible launch points which approaches closest to the target at the rear. The most favorable applications of this type of course are against slow moving targets or missiles launched from a point

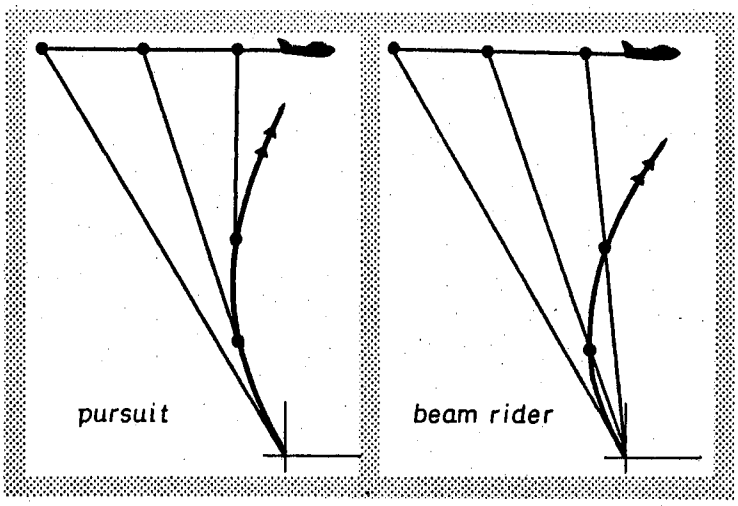

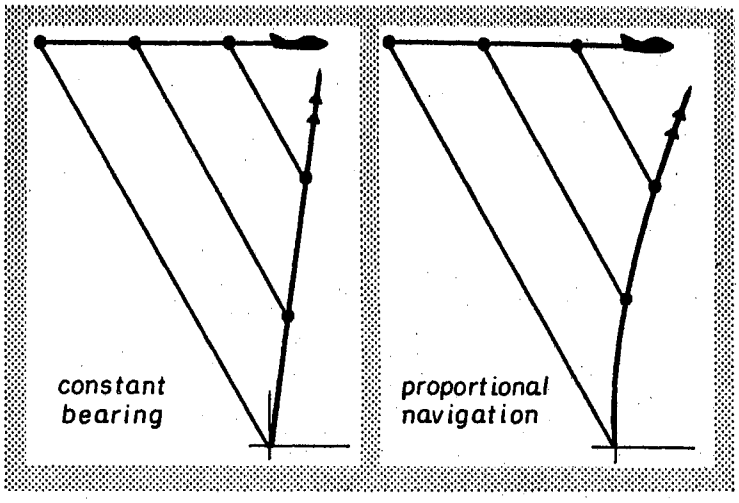

Figure 1. Typical Missile Flight Paths

to the rear of the target.

(2) Beam Rider Courses. The line of sight beam rider course is defined as that described by a missile which remains in the line of sight from a guiding point to the target. This course requires a missile acceleration less than that required for a pursuit course, but greater than the target acceleration. There are also programmed beam rider courses which differ from the line of sight type in that the beam is directed at the target during the terminal phase only. The major advantages of the beam rider course are its flexibility and the minimal complexity of the equipment which must be carried in the missile, since the major burden of guidance is assumed at the source of the beam.

(3) Constant Bearing Course. The constant bearing course (frequently called the collision course) is defined as that described by a missile moving in a manner which holds the heading of the missile-to-target line of sight constant. This course also can be defined as the straight line course to a predicted impact point. For a constant velocity target, the flight path

is a straight line. The outstanding feature of this course is that, for a maneuvering and constant speed target, the missile acceleration never exceeds the target acceleration. The major drawback lies in the fact that the weapon control system requires sufficient data gathering and data processing equipment to predict the future position of the target.

(4) Proportional Navigation Course. The proportional navigation course is defined as that described when the missile turning rate is equal to the turning rate of the missile-to-target line of sight multiplied by the navigational ratio (N). This course also can be defined as one in which the heading of the missile is equal to N times the heading at the line of sight plus a constant. When account is taken of the finite sensitivity of the control system, the two definitions lead to different paths. Values of N in the range from two to four lead to flight paths with the most desirable characteristics. Lead angles and navigation ratios usually can be chosen so that the missile acceleration will exceed the

target acceleration only slightly.

Proportional navigation was used as the guidance scheme in this research.

Proportional Guidance

The formulation of the proportional control of a missile was made in two dimensions to illustrate the proposed research. Figure 2 shows the missile, M, the target, T, and the collision point, C, for constant and unperturbed velocity. The reference frame is chosen as a matter of convenience. The vectors are defined as follows:

$$\left.\begin{aligned} \text{Missile position } \overline{M} &= X_M i + Y_M j, \\ \text{Target position } \overline{T} &= X_t i + Y_t j, \end{aligned}\right\} \qquad (1.1)$$

and Relative position $\overline{R} = \overline{T} - \overline{M} = (X_t - X_M)i + (Y_t - Y_M)j$.

Further, for the velocities

$$\left.\begin{aligned} \overline{V}_M &= \dot{X}_M i + \dot{Y}_M j, \\ \text{and} \quad \overline{V}_t &= \dot{X}_t i + \dot{Y}_M j. \end{aligned}\right\} \qquad (1.2)$$

From Figure 3, it can be seen that the line of sight angle Λ is

$$\Lambda = \text{Tan}^{-1} \frac{Y_t - Y_M}{X_t - X_M}. \qquad (1.3)$$

The missile angle is

$$\Gamma_M = \text{Tan}^{-1} \frac{\dot{Y}_M}{\dot{X}_M}. \qquad (1.4)$$

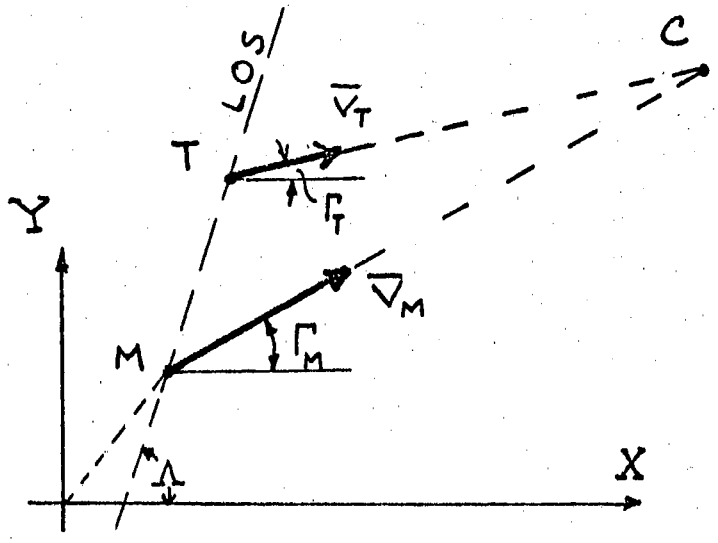

Figure 2. Collision Course

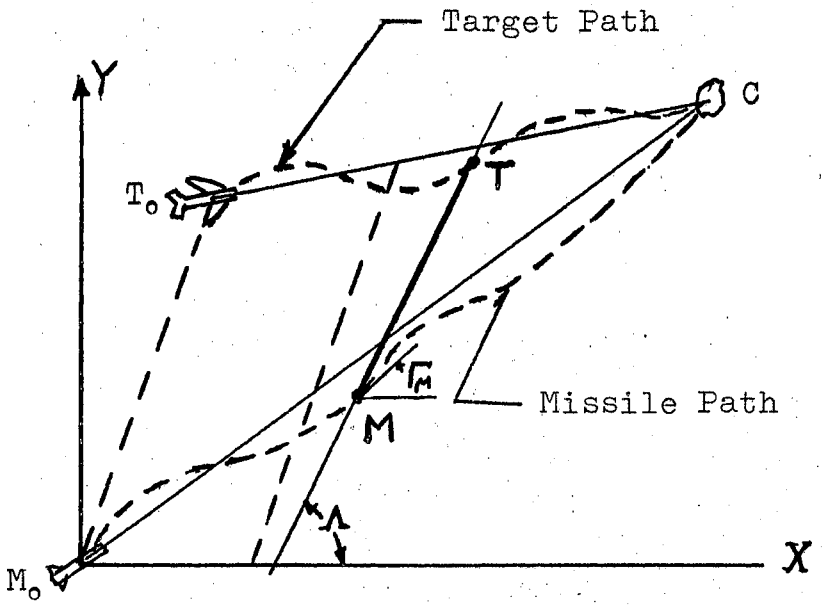

Figure 3. Coordinate System for Two-Dimensional Homing Interception

For constant velocities, the missile will collide with the target at C if $\dot{\bar{R}}$ lies along $\bar{R}$. This implies Γ_M, Γ_t, and Λ remain constant throughout the encounter. This is the constant bearing course. Proportional navigation is defined so that, as Λ changes with time, the missile, through its control system, changes its orientation, Γ, with time. Most authors use the form

$$\dot{\Gamma} = N\dot{\Lambda} \tag{1.5}$$

which implies instantaneous response of the controls (2, 3, 4, 5, and 6). A more correct statement is

$$\dot{\Gamma} = N_1 f(\dot{\Lambda}), \tag{1.6}$$

or, if the control system is linear,

$$L\{\dot{\Gamma}\} = G(s)L\{\dot{\Lambda}\}, \tag{1.7}$$

in which G(s) is the control system transfer function.

After reviewing the manner in which the perturbed motions are obtained by Merrill (4), the writer devised a method which was felt to be more mathematically correct. Essentially, it was to expand the Equations (1.1) through (1.4) concerning the constant bearing course solution in small deviations or perturbations. A Taylor Series of many variables was used resulting in

$$\gamma = \dot{y}_M \left(\frac{\text{Cos } \Gamma_{M_o}}{V_{M_o}}\right) - \dot{x}_M \left(\frac{\text{Sin } \Gamma_{M_o}}{V_{M_o}}\right) \tag{1.8}$$

and $$\lambda = \frac{\text{Cos } \Lambda_o}{R_o}\left[y_t - y_M - (x_t - x_M) \text{ Tan } \Lambda_o\right] \qquad (1.9)$$

in which the subscript, O, refers to the constant bearing course parameters and

γ is the change in the missile attitude,

λ is the change in the line of sight,

x_M and y_M are the perturbed missile coordinates, and x_t and y_t are the perturbed target coordinates. Equations (1.8) and (1.9) are linear in the perturbed variables. However, R_o approaches zero at collision, and this required special consideration in the simulation. The miss-distance was given by the perturbed variables.

Explicitly, the goals of the research proposed for this thesis were:

(1) To develop a technique for simulation of mid-course guidance which separates the missile control as a sequential sub-system.

(2) To determine miss-distance and attitude for a target which maneuvers in three dimensions; that is, essentially, to extend the state of the art to three dimensions.

CHAPTER II

SIGNIFICANT HISTORICAL CONTRIBUTIONS

Guided Missiles and Rockets

Guided missiles first became operational weapons during World War II. On August 23, 1943, German aircraft launched the HS-293 against Allied shipping in the Bay of Biscay. The weapon was a rocket-propelled, gliding bomb controlled in flight by radio command from the launching aircraft (2). The well-known V-1 (Buzz Bomb) and the V-2 (A-4) missiles, which were subsequently launched from the continent of Europe, were autopiloted missiles rather than guided missiles. The autopiloted missiles fall under a type of control known as fixed, preset, or programmed guidance, which keeps the missile on a predetermined flight path. The only Allied guided missile used during World War II was the American missile, the BAT, used against Japanese shipping in the Pacific in 1945.

Dow (2) on pages 1 through 6 has compiled an outstanding summary of the significant early history of missiles and rockets. That summary is as follows:

> Historically, the major components of advanced missiles as known today have been developed along two principal avenues: the rocket, which dates back to antiquity, and the airplane,

which has been a more modern achievement. Rockets and projectiles are considered usually to be members of the missile family, because they are fired generally along ballistic trajectories, and there are points of similarity in configuration or design. The airplane was conceived as a vehicle that would allow man to fly like a bird. As early as the year 1500, Leonardo da Vinci had envisioned a flying machine (framework), the most essential parts of which were the movable wings or oars that the pilot operated by means of stirrups and pulleys. Both concepts of design still prevail in missile development, but the distinction between the guided missile and the pilotless supersonic aircraft is vanishing rapidly. Advanced missiles and aircraft both employ moving surfaces for lift and control and similar means for propulsion; hence the differences are principally a matter of size and location of the surfaces relative to the body or fuselage. Practically all of the components for propulsion, stability, control, and guidance have become common to both.

With respect to the history of rocketry, it is recorded that Claudian, a 4th century Roman writer wrote about pyrotechnical displays which if they were not the early powder rockets, were the forerunners of them (7). Fire rockets were in use in 1232 when the Tartars fixed them in combat against the Mongols. The military applications of rockets were described in 1647 in the celebrated work Great Art of Artillery by Siemcinowitz, but this textbook was not known generally until it was translated some 80 years later by the English Board of Ordnance. The first systematic development of rockets appears to have been by William Congreve (1801), who utilized the facilities of the Royal Laboratory at Woolwich to develop models which in 1805 flew to ranges of 2000 yd or more. These weapons were used against Napoleon's forces by ships in the fleet of Sir Sidney Smith. It has been said that several hundred were fired in salvo in the attack on Boulogne. During the siege of Copenhagen (1807), the records state that some 20,000 to 40,000 rockets were employed. The Congreve rockets, like the familiar fireworks type, had long sticks for stabilization, but it was not until the time of William Hale (1846) that spin stabilization, by the jet impinging

on curved surfaces in the nozzle, was introduced to provide effective stabilization of a rocket in flight. It is interesting to note that crude attempts at guidance were made in 1405 by Eichstädt, a German engineer. He pictured in his Bellifortis a rocket traveling along a cord.

The history of jet propulsion can be traced in another direction which originated with the steam engine or aeolipile of Hero (Alexandria circa 100 B. C.) probably the first experiment to produce a gaseous jet (steam) from a liquid. Sir Isaac Newton in 1680 conceived a steam rocket to propel a carriage, and by 1855 an inventor named Phillips was working on the idea of using steam rockets for helicopters. Between 1908 and 1913, Marconnet, Coanda, and Lorin investigated the possibilities for modifying the internal-combustion engine to produce propulsion by jets. Their engines differed in concept, from the rocket of that day, in that the fuel after mixing with air was forced into the combustion chamber by a blower or compressor. Out of these developments came the air-breathing turboject, pulsejet and ramjet engines. A basic patent on modern turbojets was granted to Air Commodore Frank Whittle of the British RAF in 1930. Although the aerothermodynamic ducts (athodyds) were given intensive study by Saenger, Pabst, Walter, and Oswatitsch in Austria and Germany during World War II, the V-1 pulsejet of Paul Schmidt and W. Kamm was the only engine of this type to become operational during that period. The first successful ramjet was not demonstrated in flight until postwar days when the Applied Physics Laboratory of Johns Hopkins University, working under contract with the Bureau of Ordnance, U. S. Navy, flight-tested over a range of 12,000 yd a 6-in. supersonic model (Flying Stovepipe) that developed a thrust in excess of drag resistance. One of these early test vehicles was presented by the Bureau of Ordnance to the National Air Museum of the Smithsonian Institution.

Looking now at the history of man's flight, it is seen that gliding and soaring became successful only in relatively modern times. Although Sir Hiram Maxim, Chanute, Langley, and others rendered significant contributions to the art of flying late in the nineteenth century, it remained for the Wright Brothers to first

demonstrate in 1900 the feasibility of aerodynamic control of a powered vehicle in flight. In 1910 Elmer A. Sperry and H. C. Ford installed a gyroscopic stabilizer in an airplane, and by 1914 the automatic control of aircraft had been achieved. The rapid progress of radio after World War I soon led to successful applications for the control of aircraft, and by 1920 radio control of pilotless aircraft (drones) had progressed to the point where the U. S. Armed Forces were able to demonstrate the possibilities of command guidance. As early as 1925, Breit and Tuve in the United States had showed the possibilities of pulse ranging, and in 1939 the potentialities of pulse radar were confirmed by tests aboard the USS New York. The unparalleled activity in electronics during World War II firmly established radar as a basic technique for recognizing, acquiring, and tracking a moving target.

Coincidental with the development of the airplane the late Professor Robert H. Goddard (8) had carried on, practically single-handedly, a series of experimental and theoretical studies that established the practicability of the liquid-propellant rocket. His writings on the subject began in 1907 when he was beginning to speculate on means of studying the upper atmosphere, and in 1914 he was able to initiate a modest experimental program which was to continue without serious interruption until the time of his death. A brilliant physicist, possessing indefatigable determination and unusual patience, he was the first investigator to approach rocket design in a methodical and thoroughly scientific manner. The difficulties that he faced are aptly summarized by the editors of his paper (9):

'The enormous volume of work he accomplished during his lifetime is the more remarkable, in view of the fact that he was a lifelong sufferer from tuberculosis, which became manifest in early manhood. Not only was there ill health to combat, but he was hampered by lack of sufficient funds during a large part of his productive life. Added to this was the constant skepticism of the technical world toward rockets, and the sensational, distorted publicity and ridicule that from time to time burst into the press. None-theless, his cheerful and gay spirit marked his life as a happy one.'

Meanwhile, a German contemporary of Goddard, Professor Hermann von Oberth, independently had aroused considerable enthusiasm in rocketry by his Die Rakete zu Planetenraumen in 1923, followed by Wege zu Raumschiffahrt, for which he was granted the Esnault-Pelterie and Hirsh award of the Societe' Astronomique in 1928. He was instrumental in organizing the Verein fur Raumschiffahrt (VfR), a popular rocket society, which was probably responsible in part for the decision of the German Army in 1929 to develop the rocket as a combat weapon. In 1930 Captain Walter Dornberger, later Major General in charge of V-2 development at Peenemuende, joined the Army's program which was then directed toward liquid-propellant rockets (10). Late in 1934 Dornberger's group was flight-testing liquid fuel rockets on an island in the North Sea (Borkum), moving eventually to Peenemuende which was established in the summer of 1940. During this period Max Vallier of Munich was conducting tests with a rocket-propelled automobile. The American Interplanetary Society, later the American Rocket Society, was established in 1930, but there was no sustained interest in the United States until World War II when German solid-propellant artillery rockets, the V-1 and the V-2 were directed against the Allies.

The first flight of a liquid-oxygen-gasoline rocket occurred on March 16, 1926, at Auburn, Mass., a distance of 184 ft. being traveled in 25 sec. This was essentially a small combustion chamber and nozzle located several feet ahead of the fuel tanks, and connected to them by two pipes which also furnished structural support. On July 17, 1929, an improved rocket, about 57 lb. weight at launching and with the combustion chamber at the rear, carried a thermometer, an aneroid barometer, a camera (to photograph readings), and a parachute to an altitude of 90 ft., over a horizontal range of 171 ft. In subsequent flights at Roswell, N. M., Professor Goddard demonstrated flight stabilization by means of jet and air vanes controlled by a gyroscope, the first successful test being recorded on March 25, 1935. Successive corrections of the flight path were obtained during a vertical rise of several hundred feet. In 1937 steering was accomplished by means of a pivoted tailpiece which carried the combustion chamber. Just before engaging in military activities, in the

fall of 1941, Dr. Goddard was employing fuel pumps (turbines) and experimenting with methods of fuel injection. His experimental rocket of this period was about 18 in. in diameter, nearly 22 ft. long, and weighed approximately 500 lb. at launching.

Mid-Course Guidance

Early methods of mid-course guidance were explored by Newell (11) in which he compared the results of pursuit courses, constant bearing courses, and the then new proportional course. In the latter case, the equations were solved sequentially by numerical techniques.

The most comprehensive treatment of the subject is in the series edited by Merrill (3 and 4). This series includes all phases of guided missile design, and attempts to unify somewhat the notation in the field. This thesis will use Merrill's notation as much as possible.

Some publications present the mathematical relationships for the flight paths in a rigorous manner (5, 12, and 13). However, the missile dynamic response to command changes are not treated as thoroughly. Conversely, others are more concerned with the missile dynamic response (14, 15, and 16).

An example of two-dimensional simulation of proportional navigation is given by Rogers and Connelly (6, pp. 370-377).

Finally, a general source is a reference textbook prepared for use at the U. S. Naval Academy (1).

Adequate published information on mid-course guidance

is given in references (1) through (16) in which Merrill (3) and (4), Clemow (5), and Newell (11) delve deepest into theoretical analysis. With the target and missile initially on a collision course (Figure 3), the deviations from the paths are considered as a two-dimensional problem.

Analyses have been carried out for the missile deviation from missile reference course, z_M, in which initial missile heading error, or target heading error, or target maneuver is the input (4). The combination of all inputs has not been analyzed.

A simulation has been made for an idealized two-dimensional case (6).

In all cases, there are questionable assumptions in determining the rate of change in the line of sight.

In summarizing the literature pertinent to the research of this thesis, the following general conclusions are made from the unclassified literature currently available:

(1) The analyses are primarily in two-dimensions whereas target maneuver occurs in three-dimensions, or, more specifically, out of the reference course plane.

(2) The analyses are not comprehensive enough to account for all possible errors in the same analysis.

(3) The analyses are based on questionable

if not, in some cases, erroneous assumptions concerning the treatment of the missile dynamics.

CHAPTER III

KINEMATIC ANALYSIS OF MISSILE AND TARGET ENCOUNTER

Reference Systems

The missile and target geometry shown in Figures 2 and 3 are adequate for a two-dimensional encounter, but need to be revised for three dimensions. Figures 4 and 5 represent the three-dimensional encounter.

Figure 4 shows the collison course of the missile and target identified by the plane containing the points O, T_o, M_o, T_1, and M_1, and the angles Λ_o, Γ_{Mo}, L, Γ_{to}, and A. If no changes in target or missile heading or position occur, the missile and target would be located at points M_1 and T_1 after a time t_1. These positions are the end-points of the vector $\bar{R}_1$ which lies in the collision course plane and is parallel to $\bar{R}_o$. Collision would occur at time t_c in that plane. However, at t_1 the missile and target have maneuvered to points M and T which generally are not in the collision course plane, resulting in a rotation of the relative position vector $\bar{R}$. The missile velocity vector $\dot{\bar{M}}$ must be rotated simultaneously to accomplish intercept.

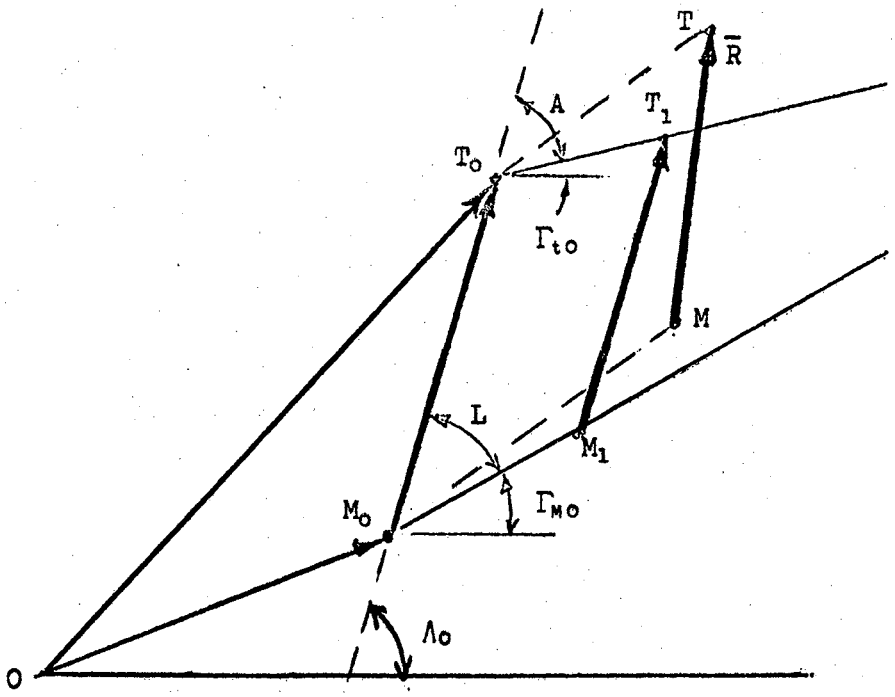

Figure 4. Missile and Target Geometry

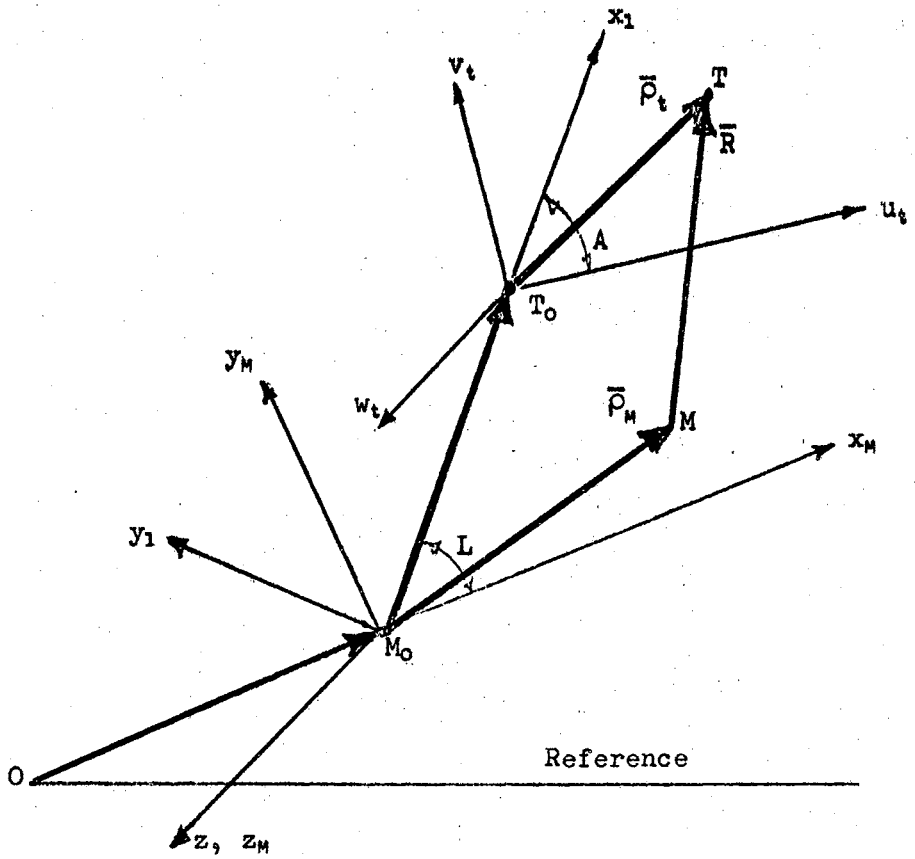

Figure 5. Coordinate Systems and Axes

Figure 5 shows the coordinate systems to be used herein. The x_1, y_1, and z axes form a triad with x_1 along the original line of sight and z perpendicular to the collision course plane. The x_M, y_M, z_M triad is located at M_o, with the x_M axis along the missile collision course. The u_t, v_t, w_t triad is located at T_o, with the u_t axis along the target collision course and the w_t axis perpendicular to the collision course plane. Thus, w_t and z_M are parallel.

At the start of mid-course guidance ($t = 0$), the target and missile are assumed to be in the positions $\bar{T}_o$ and $\bar{M}_o$ with heading angles Γ_{to} and Γ_{Mo}, respectively. At some later time, they are in positions $\bar{T}$ and $\bar{M}$ which are off the predicted collision course. The line of sight vector has changed from $\bar{R}_o$ to $\bar{R}$, and not to the predicted value, $\bar{R}_1$. The first concern is to obtain the rate of change of the direction of the line of sight, $\bar{R}$, and to relate it to the rate of change of the direction of the missile velocity, $\dot{\bar{M}}$.

Range and Range Rate Equations

From the reference point O, the target position is

$$\bar{T} = \bar{T}_o + \bar{\rho}_t . \qquad (3.1)$$

The missile position is

$$\bar{M} = \bar{M}_o + \bar{\rho}_M . \qquad (3.2)$$

The relative position $\bar{R}$ is the range vector, whose

direction is the line of sight. This vector is

$$\bar{R} = \bar{T} - \bar{M} = \bar{R}_o + \bar{\rho}_t - \bar{\rho}_M, \tag{3.3}$$

where

$$\bar{R}_o = \bar{T}_o - \bar{M}_o. \tag{3.4}$$

These vectors are expressed in terms of their unit vectors as follows:

$$\bar{R}_o = R_o I; \tag{3.5}$$

$$\bar{\rho}_M = x_M i + y_M j + z_M k; \tag{3.6}$$

and

$$\bar{\rho}_t = u_t \varepsilon_1 + v_t \varepsilon_2 + w_t k, \tag{3.7}$$

where I, J, and K are unit vectors along x_1, y_1, z; i, j, and k are unit vectors along x_M, y_M, z_M, and ε_1, ε_2, and k are unit vectors along u_t, v_t, and w_t axes. The objective is to express $\bar{R}$ in a convenient form. Therefore, $\bar{\rho}_t$ and ρ_M will be transformed to the line of sight reference by using Equation (AA.4) from Appendix A. Thus,

$$\bar{\rho}_t = [u_t \text{ Cos } A + v_t \text{ Sin } A]I + [-u_t \text{ Sin } A + v_t \text{ Cos } A]J + w_t K, \tag{3.8}$$

and

$$\bar{\rho}_M = [x_M \text{ Cos } L + y_M \text{ Sin } L]I + [-x_M \text{ Sin } L + y_M \text{ Cos } L]J + z_M K. \tag{3.9}$$

Using Equations (3.5), (3.8), and (3.9) in (3.3), there results

$$\bar{R} = R_X I + R_Y J + R_Z K, \tag{3.10}$$

in which

$$R_x = R_o + u_t \text{ Cos } A + v_t \text{ Sin } A - x_M \text{ Cos } L - y_M \text{ Sin } L,$$

$$R_y = -u_t \text{ Sin } A + v_t \text{ Cos } A + x_M \text{ Sin } L - y_M \text{ Cos } L,$$

and $$R_Z = w_t - z_M . \qquad (3.11)$$

The subscripts x, y, and z refer to the line of sight reference axes x_1, y_1, and z. The range R may be expressed in cylindrical coordinates by using Equation (AA.8), as follows:

$$\bar{R} = R\, \varepsilon_R , \qquad (3.12)$$

resulting in

$$R_x = R \text{ Cos } \varphi_R \text{ Cos } \theta_R ,$$

$$R_y = R \text{ Cos } \varphi_R \text{ Sin } \theta_R , \qquad (3.13)$$

and $$R_Z = R \text{ Sin } \varphi_R .$$

These vectors are shown in Figure 6, which is similar to Figure 25 with the subscript R used to identify the range vector.

The relative velocity (range rate), $\dot{\bar{R}}$, is found by differentiating Equation (3.10), yielding

$$\dot{\bar{R}} = \dot{R}_x I + \dot{R}_y J + \dot{R}_Z K . \qquad (3.14)$$

From Equation (AA.9), an alternate expression is

$$\dot{\bar{R}} = \dot{R}\, \varepsilon_R + R\ \dot{\theta}_R \text{ Cos } \varphi_R\, \varepsilon_{\theta R} + R\, \dot{\varphi}_R\, \varepsilon_{\varphi R} , \qquad (3.15)$$

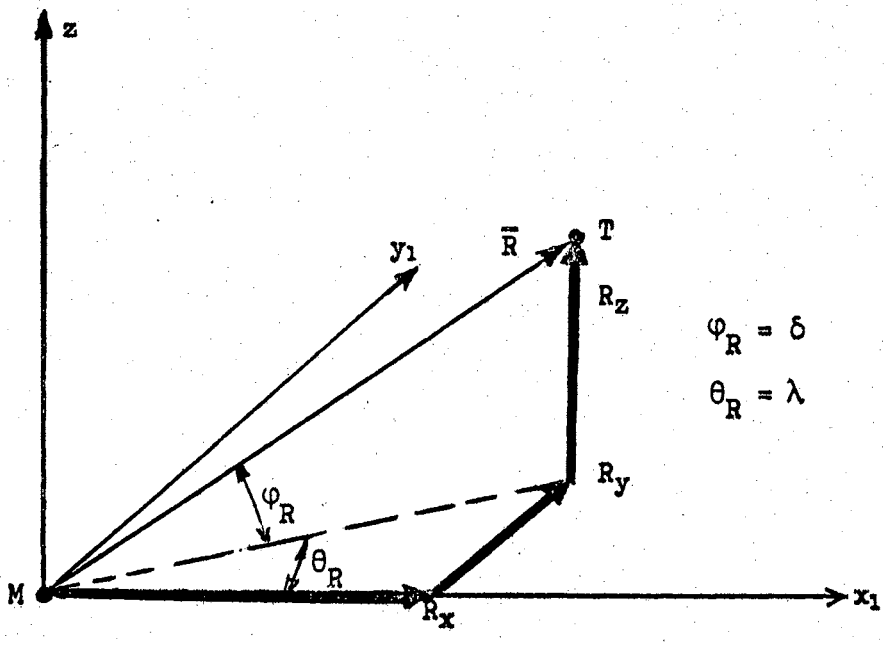

Figure 6. Range Vector, $\bar{R}$

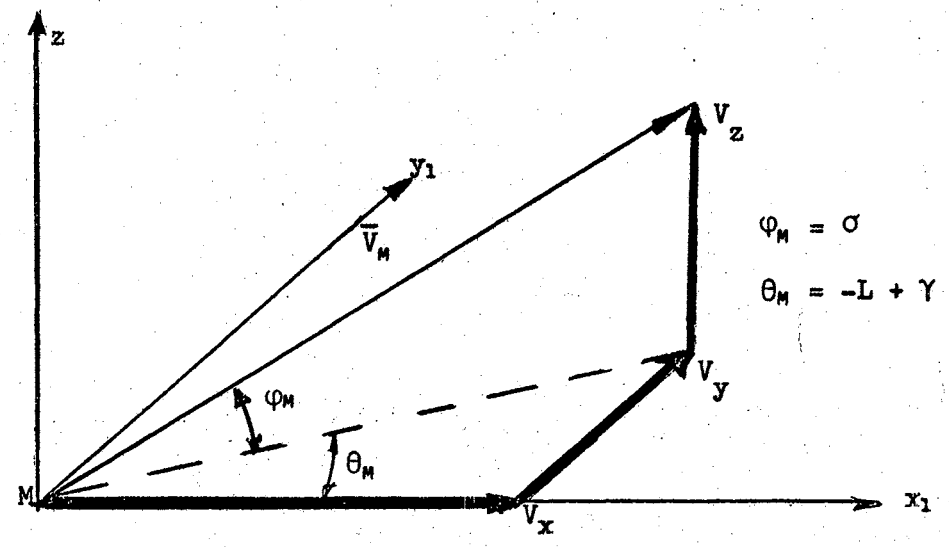

Figure 7. Missile Velocity, $\bar{V}_M$

in which $\dot{R}$ is the change in R along ε_R, and R is given by

$$R = \left\{R_x^2 + R_y^2 + R_z^2\right\}^{\frac{1}{2}}. \tag{3.16}$$

Using the components of the vector $\dot{\bar{R}}$ given by Equations (3.14) and (3.15) and the transformation Equation (AA.7), there results,

$$\dot{R} = \dot{R}_x \text{ Cos } \varphi_R \text{ Cos } \theta_R + \dot{R}_y \text{ Cos } \varphi_R \text{ Sin } \theta_R + \dot{R}_z \text{ Sin } \varphi_R,$$

$$R\dot{\theta}_R \text{ Cos } \varphi_R = -\dot{R}_x \text{ Sin } \theta_R + \dot{R}_y \text{ Cos } \theta_R$$

and

$$R\,\dot{\varphi}_R = -\dot{R}_x \text{ Sin } \varphi_R \text{ Cos } \theta_R - \dot{R}_y \text{ Sin } \varphi_R \text{ Sin } \theta_R + \dot{R}_z \text{ Cos } \varphi_R. \tag{3.17}$$

Further from Equation (3.11),

$$\dot{R}_x = \dot{u}_t \text{ Cos A} + \dot{v}_t \text{ Sin A} - \dot{x}_M \text{ Cos L} - \dot{y}_M \text{ Sin L},$$

$$\dot{R}_y = -\dot{u}_t \text{ Sin A} + \dot{v}_t \text{ Cos A} + \dot{x}_M \text{ Sin L} - \dot{y}_M \text{ Cos L},$$

and

$$\dot{R}_z = \dot{w}_t - \dot{z}_M. \tag{3.18}$$

Equations (3.17) can be expressed in a more convenient form by substitution of Equations (3.13) resulting in

$$\dot{R} = \frac{1}{R}\left[R_x \dot{R}_x + R_y \dot{R}_y + R_z \dot{R}_z\right],$$

$$\dot{\theta}_R = \frac{1}{R_x^2 + R_y^2}\left[-\dot{R}_x R_y + \dot{R}_y R_x\right] \tag{3.19}$$

and

$$\dot{\varphi}_R = \frac{1}{R^2\sqrt{R_x^2 + R_y^2}}\left[R_z(-\dot{R}_x R_x - \dot{R}_y R_y) + \dot{R}_z(R_x^2 + R_y^2)\right]$$

The Equations (3.19) represent the range rate and the changes in the range vector (line of sight). They are related to the missile and target coordinates by Equations (3.11) and (3.18). An alternate method for obtaining Equations (3.19) is to differentiate (3.13). The results are identical, providing a check on the derivation.

Missile Velocity

In the missile coordinates, the missile velocity is given as

$$\bar{V}_M = \dot{x}_M i + \dot{y}_M j + \dot{z}_M k, \qquad (3.20)$$

which is transformed to the line of sight coordinates by a rotation through an angle L, using Equations (AA.4). The resulting expression is

$$\bar{V}_M = V_X I + V_Y J + V_Z K, \qquad (3.21)$$

in which

$$V_X = \dot{x}_M \text{ Cos } L + \dot{y}_M \text{ Sin } L,$$

$$V_Y = -\dot{x}_M \text{ Sin } L + \dot{y}_M \text{ Cos } L,$$

and

$$V_Z = \dot{z}_M. \qquad (3.22)$$

Figure 7 shows the missile vector resolved along the original line of sight coordinates. Proceeding, as before, with

$$\bar{V}_M = V_M \varepsilon_{VM} \qquad (3.23)$$

where

$$V_M = \left\{V_X^2 + V_Y^2 + V_Z^2\right\}^{\frac{1}{2}}, \tag{3.24}$$

then, using Equation (AA.9), there results

$$\dot{\bar{V}}_M = \dot{V}_M \varepsilon_{V^M} + V_M \dot{\theta}_M \operatorname{Cos} \varphi_M \varepsilon_{\theta_M} + V_M \dot{\varphi}_M \varepsilon_{\varphi_M}. \tag{3.25}$$

In the x_1, y_1, z reference,

$$\dot{\bar{V}}_M = \dot{V}_X I + \dot{V}_Y J + \dot{V}_Z K, \tag{3.26}$$

where

$$\dot{V}_X = \ddot{x}_M \operatorname{Cos} L + \ddot{y}_M \operatorname{Sin} L,$$

$$\dot{V}_Y = -\ddot{x}_M \operatorname{Sin} L + \ddot{y}_M \operatorname{Cos} L,$$

and $$\dot{V}_Z = \ddot{z}_M. \tag{3.27}$$

Transforming (3.25), using Equations (AA.7), (3.22), and (3.27), there results:

$$\dot{V}_M = \dot{V}_X \operatorname{Cos} \varphi_M \operatorname{Cos} \theta_M + \dot{V}_Y \operatorname{Cos} \varphi_M \operatorname{Sin} \theta_M + \dot{V}_Z \operatorname{Sin} \varphi_M,$$

$$V_M \dot{\theta}_M \operatorname{Cos} \varphi_M = -\dot{V}_X \operatorname{Sin} \theta_M + \dot{V}_Y \operatorname{Cos} \theta_M,$$

and $$V_M \dot{\varphi}_M = -\dot{V}_X \operatorname{Sin} \varphi_M \operatorname{Cos} \theta_M - \dot{V}_Y \operatorname{Sin} \varphi_M \operatorname{Sin} \theta_M + \dot{V}_Z \operatorname{Cos} \varphi_M. \tag{3.28}$$

These are analogous to Equations (3.17), and can be further simplified in a like manner. In cylindrical coordinates the velocity is

$$V_X = V_M \operatorname{Cos} \varphi_M \operatorname{Cos} \theta_M,$$

$$V_Y = V_M \text{ Cos } \varphi_M \text{ Sin } \theta_M ,$$

and $$V_Z = V_M \text{ Sin } \varphi_M , \qquad (3.29)$$

which, when substituted into (3.28), yields

$$\dot{V}_M = \frac{1}{V_M}\left[\dot{V}_X V_X + \dot{V}_Y V_Y + \dot{V}_Z V_Z\right],$$

$$\dot{\theta}_M = \frac{1}{V_X^2 + V_Y^2}\left[-\dot{V}_X V_X + \dot{V}_Y V_Y\right],$$

and $$\dot{\varphi}_M = \frac{1}{V_M^2\sqrt{V_X^2 + V_Y^2}}\left[V_Z(-\dot{V}_X V_X - \dot{V}_Y V_Y) + \dot{V}_Z(V_X^2 + V_Y^2)\right].$$

(3.30)

Equations (3.30) represent the missile speed change and the direction changes of the velocity. θ_M is in the same plane as θ_R (the collision plane), and φ_M and φ_R are in planes perpendicular to the collision plane; however, they are not in the same plane.

Proportional Navigation

The principle of proportional navigation is to make the turning rate of the missile ($\dot{\theta}_M$ and $\dot{\varphi}_M$) proportional to the the turning rate of the line of sight ($\dot{\theta}_R$ and $\dot{\varphi}_R$). This can only be done by commanding the missile to respond through inputs $\dot{\theta}_R$ and $\dot{\varphi}_R$. After some time, depending on the missile response, a new missile course is established. These conditions are expressed mathematically as:

$$\dot{\theta}_M = f_1(\dot{\theta}_R, \dot{\varphi}_R),$$

$$\dot{\varphi}_M = f_2(\dot{\theta}_R, \dot{\varphi}_R), \qquad (3.31)$$

in which f_1 and f_2 represent the dynamic response of the missile, including the coupling between the yaw and pitch modes. For the sake of clarity, the θ_M direction will be called the yaw mode and the φ_M direction will be called the pitch mode.

Most authors treat the two modes as having identical transfer functions, and this assumption will be made herein. This assumption is reasonable, and has little bearing on the main objective, which is to verify the encounter simulation. In fact, an ideal transfer function, representing a well designed guidance system, will be assumed.

Missile Transfer Function

The missile transfer functions selected for use in this research conform to good design practices of automatic control (20) and (21). Regardless of the open loop transfer function, the system is compensated so that the dominant poles give a response closely approximated by a second order system. To prevent involvement in the problem of designing an automatic control system, the desired result was assumed. That is, a second order transfer function was assumed.

The transfer function selected for yaw was

$$\frac{L\{\dot{\theta}_M\}}{L\{\dot{\theta}_R\}} = \frac{3(0.333)}{s^2 + 0.587s + 0.333}. \qquad (3.32)$$

The pitch transfer function was identical. The response

of Equation (3.32) to a unit step function yields the following performance criteria:

1. The final value is 3 which is the navigation ratio found reasonable (2), (4), and (6).
2. The system approaches within 2% of its final value within 14 seconds which is within the minimum time of collision course.
3. The equivalent time constant is within 0.1 t_c as recommended by Merrill (4) on page 93. The t_c was for a tail chase (A = 0).

The system is still rather sluggish for the more direct attack angles ($45° < A < 180°$); however, to speed up the response would have caused considerable scaling problems in the analog program. The experimental results, particularly the calibration runs, show that the yaw and pitch transfer functions respond satisfactorily, and, therefore, the transfer function needs no further modification.

Nonlinear System

The foregoing system of equations is adequate to simulate the missile encounter with the target. However, the nonlinear nature of those equations requires a large number of multipliers and other analog components, beyond the capability of the available analog computer. To

simulate the system of nonlinear equations, some linearization, or approximation, was necessary.

Linearization of Equations

The guidance equations are nonlinear in the missile and target positions and their derivatives. These equations can be linearized, using perturbations from the collision course. This was accomplished by use of a Taylor series expansion about the collision course solution. Using an expansion of the form

$$F(x_1 + h_1, x_2 + h_2, \ldots, x_n + h_n) = F_1(x_1, x_2, x_3, \ldots, x_n) + \sum_{i=1}^{n} a_i x_i + \text{H.O.T.} \tag{3.33}$$

where the higher order terms (H.O.T.) are assumed negligible. The first term on the right is the collision course solution, and the series a_i coefficients are, simply:

$$a_i = \frac{\partial F}{\partial x_i} \tag{3.34}$$

evaluated where all the h perturbation variables are zero. If a notation

$$F = F_1 + F_p \tag{3.35}$$

is used, then the subscript 1 refers to the collision course solution, and p is the perturbed or linearized solution

$$F_p = \sum_{i=1}^{n} a_i x_i . \tag{3.36}$$

When each variable is expanded, as described in the foregoing, the following results are obtained.

For the missile:

$$x_M = X_1 + x, \tag{3.37}$$

$$\dot{x}_M = V_{M0} + \dot{x}, \tag{3.38}$$

in which

$$X_1 = V_{M0} t. \tag{3.39}$$

Further,

$$y_M = 0 + y, \; \dot{y}_M = \dot{y}, \tag{3.40}$$

and

$$z_M = 0 + z, \; \dot{z}_M = \dot{z}. \tag{3.41}$$

The missile directions are

$$\theta_M = -L + \gamma \quad , \quad \dot{\theta}_M = \dot{\gamma} \; , \tag{3.42}$$

and

$$\varphi_M = 0 + \sigma \quad , \quad \dot{\varphi}_M = \dot{\sigma} \; . \tag{3.43}$$

For the target:

$$u_t = U_1 + u, \tag{3.44}$$

$$\dot{u}_t = V_{t0} + \dot{u}, \tag{3.45}$$

in which

$$U_1 = V_{to}\, t. \tag{3.46}$$

Further

$$v_t = 0 + v \quad , \quad \dot{v}_t = \dot{v}, \tag{3.47}$$

and

$$w_t = 0 + w \quad , \quad \dot{w}_t = \dot{w}. \tag{3.48}$$

For the relative position (range):

$$\theta_R = 0 + \lambda \text{ and } \dot{\theta}_R = \dot{\lambda} \quad ; \tag{3.49}$$

$$\varphi_R = 0 + \delta \text{ and } \dot{\varphi}_R = \dot{\delta} \quad ; \tag{3.50}$$

$$R_x = R_{x1} + R_{xp} \; ;$$

$$R_{x1} = R_o + U_1 \text{ Cos } A - X_1 \text{ Cos } L \; ; \tag{3.51}$$

$$R_{xp} = u \text{ Cos } A + v \text{ Sin } A - x \text{ Cos } L - y \text{ Sin } L \; ; \tag{3.52}$$

$$R_y = R_{y1} + R_{yp} \; ;$$

$$R_{y1} = - U_1 \text{ Sin } A + X_1 \text{ Sin } L = 0 \; ; \tag{3.53}$$

$$R_{yp} = - u \text{ Sin } A + v \text{ Cos } A + x \text{ Sin } L - y \text{ Cos } L \; ; \tag{3.54}$$

$$R_Z = R_{Zp} = w - z, \tag{3.55}$$

and

$$R = R_{x1}. \tag{3.56}$$

For the range rate, the components are found by differentiating the range components. This results in

$$\dot{R}_{x1} = -[V_{Mo}\ \text{Cos}\ L - V_{to}\ \text{Cos}\ A]\ ,\ \dot{R}_{x1} < 0\ ;$$

$$\dot{R}_1 = \dot{R}_{x1}\ , \tag{3.57}$$

and

$$\dot{R}_{y1} = -V_{to}\ \text{Sin}\ A + V_{Mo}\ \text{Sin}\ L = 0. \tag{3.58}$$

Further, $\dot{R}_{xp}$, $\dot{R}_{yp}$, and $\dot{R}_{zp}$ are found from (3.52), (3.54), and (3.55) by differentiation.

One more expression is obtained from Equation (3.51) using (3.57)

$$R_1 = R_{x1} = R_o - [V_{Mo}\ \text{Cos}\ L - V_{to}\ \text{Cos}\ A]t. \tag{3.59}$$

Equations (3.19) are linearized to yield:

$$\dot{R}_p = \dot{R}_{xp} = \dot{u}\ \text{Cos}\ A + \dot{v}\ \text{Sin}\ A - \dot{x}\ \text{Cos}\ L - \dot{y}\ \text{Sin}\ L\ ;$$

$$\dot{\theta}_{RP} = \dot{\lambda} = \frac{d}{dt}\left[\frac{R_{yp}}{R_1}\right]\ , \tag{3.60}$$

$$\dot{\varphi}_{RP} = \dot{\delta} = \frac{d}{dt}\left[\frac{R_{zp}}{R_1}\right]\ . \tag{3.61}$$

and

$$\dot{\varphi}_{RP} = \dot{\delta} = \frac{d}{dt}\left[\frac{R_{zp}}{R_1}\right]\ . \tag{3.62}$$

It should be noted here that R_1 is a function of time given by Equation (3.59), and, thereby, the ordinary differential equations found by this linearization procedure have time varying coefficients.

The missile components are referenced to the original line of sight by Equations (3.20) through (3.30). The linearized system is as follows:

$$V_{x1} = V_{M0} \text{ Cos } L, \; V_{y1} = - V_{M0} \text{ Sin } L \; ; \tag{3.63}$$

$$V_{xp} = \dot{x} \text{ Cos } L + \dot{y} \text{ Sin } L \; ; \tag{3.64}$$

$$V_{yp} = -\dot{x} \text{ Sin } L + \dot{y} \text{ Cos } L \; ; \tag{3.65}$$

$$V_{zp} = \dot{z} \; ; \tag{3.66}$$

$$\dot{V}_{xp} = \ddot{x} \text{ Cos } L + \ddot{y} \text{ Sin } L \; ; \tag{3.67}$$

$$\dot{V}_{yp} = -\ddot{x} \text{ Sin } L + \ddot{y} \text{ Cos } L \; , \tag{3.68}$$

and

$$\dot{V}_{zp} = \ddot{z} \; . \tag{3.69}$$

Further

$$\dot{V}_{Mp} = \ddot{x} \; ; \tag{3.70}$$

$$\dot{\theta}_{Mp} = \dot{\gamma} = \frac{\ddot{y}}{V_{M0}} \; , \tag{3.71}$$

and

$$\dot{\varphi}_{Mp} = \dot{\sigma} = \frac{\ddot{z}}{V_{M0}} \; . \tag{3.72}$$

Nonlinear Approximate Equations

During the experimental phase of this research, it became necessary to modify the linearized system to properly calculate the $\dot{x}$ component of the missile and to simulate the turning rates $\dot{\lambda}$ and $\dot{\delta}$.

The first modification was in Equation (3.70) for calculating $\ddot{x}$ and thereby $\dot{x}$. Equation (3.70) results from the first of Equations (3.30) which, in itself, is the differentiation of

$$V_M^2 = (V_{M0} + \dot{x})^2 + \dot{y}^2 + \dot{z}^2 \tag{3.73}$$

in a more complicated form. Thus, $\dot{x}$ can be found as

$$\dot{x} = -V_{M_0} + \sqrt{V_M^2 - \dot{y} - \dot{z}^2}. \qquad (3.74)$$

As will be shown by the analog computer results, the linearized relationships for λ and δ were adequate for heading and position errors. However, when the target was maneuvering continually, in a manner which gave $R_{x1} < 0$ when $R_x > 0$, the simulation was not as effective as in the prior cases. A better approximation was required.

Consider Equations (3.13). The first two yield

$$\text{Tan } \theta_R = \frac{R_y}{R_x} , \qquad (3.75)$$

from which for small angles

$$\theta_R = \lambda = \frac{R_y}{R_x} , \qquad (3.76)$$

where $R_y = R_{yp}$ and $R_x = R_{x1} + R_{xp}$.

In a like manner, φ_R is found from Equations (3.13) to be

$$\varphi_R = \delta = \text{Tan}^{-1} \frac{R_z}{\sqrt{R_x^2 + R_y^2}} \qquad (3.77)$$

with the small angle approximation,

$$\delta = \frac{R_z}{R_x} . \qquad (3.78)$$

When these were used for the target maneuver the missile exhibited a more stable flight.

The pure nonlinear simulation was not attempted due to lack of working computer components.

CHAPTER IV

ANALOG COMPUTER SIMULATION

Unscaled System

The system of unscaled equations which were finally used in the experiments, discussed in the next chapter, will now be presented. Equations (3.8) and (3.9), using (3.3), yield (3.11) and, eventually, (3.51) through (3.56).

From Equations (3.8) and (3.9), using the notation subsequent to (3.33), there results:

$$\rho_{tx} = [V_{t_o} \text{ Cos } A]t + u \text{ Cos } A + v \text{ Sin } A, \qquad (4.1)$$

from integration of

$$\dot{\rho}_{tx} = V_{t_o} \text{ Cos } A + \dot{u} \text{ Cos } A + \dot{v} \text{ Sin } A. \qquad (4.2)$$

The missile x coordinate is

$$\rho_{mx} = [V_{m_o} \text{ Cos } L]t + x \text{ Cos } L + y \text{ Sin } L, \qquad (4.3)$$

from integration of

$$\dot{\rho}_{mx} = V_{m_o} \text{ Cos } L + \dot{x} \text{ Cos } L + \dot{y} \text{ Sin } L. \qquad (4.4)$$

Further,

$$R_x = R_o + \rho_{tx} - \rho_{Mx}, \tag{4.5}$$

which is the same as the sum of Equations (3.51) and (3.52).

The y components are

$$\rho_{ty} = -[V_{to} \text{ Sin } A]t - u \text{ Sin } A + v \text{ Cos } A \tag{4.6}$$

and

$$\dot{\rho}_{ty} = -V_{to} \text{ Sin } A - \dot{u} \text{ Sin } A + \dot{v} \text{ Cos } A, \tag{4.7}$$

for the target. The missile position is

$$\rho_{My} = -[V_{Mo} \text{ Sin } L]t - x \text{ Sin } L + y \text{ Cos } L, \tag{4.8}$$

and its velocity is

$$\dot{\rho}_{My} = - V_{Mo} \text{ Sin } L - \dot{x} \text{ Sin } L + \dot{y} \text{ Cos } L. \tag{4.9}$$

Further,

$$R_y = \rho_{ty} - \rho_{My}, \tag{4.10}$$

as verified by Equations (3.53) and (3.54).

The z components are

$$\rho_{tz} = w, \tag{4.11}$$

$$\dot{\rho}_{tz} = \dot{w}, \tag{4.12}$$

$$\rho_{Mz} = z, \tag{4.13}$$

$$\dot{\rho}_{Mz} = \dot{z}, \tag{4.14}$$

and

$$R_z = \rho_{tz} - \rho_{Mz}, \tag{4.15}$$

as given by Equation (3.55).

From Equation (3.59),

$$R_1 = R_o + \dot{R}_{x1}\, t, \tag{4.16}$$

in which

$$\dot{R}_{x1} = -\left[V_{Mo} \cos L - V_{to} \cos A\right]. \tag{4.17}$$

The preceding seventeen equations are presented somewhat out of the natural order derived in Chapter III. However, they are in logical order for programming on the computer.

The line of sight turning rates are given by Equation (3.61) and (3.62), which are solved and placed in the form for programming as follows:

$$\lambda = \frac{1}{R_o}\left[(-R_{x1}\, t)\lambda + R_Y - R_{Yo}\right], \tag{4.18}$$

and

$$\delta = \frac{1}{R_o}\left[(-R_{x1}\, t)\delta + R_Z - R_{Zo}\right]. \tag{4.19}$$

The missile yaw and pitch dynamics are given by the transfer function of Equation (3.32). This represents:

$$\dddot{\theta}_M + 0.587\ddot{\theta}_M + 0.333\dot{\theta}_M = \dot{\theta}_R,$$

or, by integrating once and substituting (3.42),

$$\ddot{Y} + 0.587\dot{Y} + 0.333Y = \lambda, \tag{4.20}$$

where

$$\theta_M = -L + Y. \tag{4.21}$$

For φ_M, using Equation (3.43), there results:

$$\ddot{\sigma} + 0.587\dot{\sigma} + 0.333\sigma = \delta. \tag{4.22}$$

Another equation to be used in the program is the missile speed compatibility, Equation (3.74), which is repeated here, for completeness, as:

$$\dot{x} = -V_{M_O} + \sqrt{V_M^2 - \dot{y}^2 - \dot{z}^2}. \tag{4.23}$$

In this analysis, the missile speed is assumed constant. Thus,

$$V_M = V_{M_O}, \tag{4.24}$$

and $\dot{x}$ is always negative.

The other missile velocity components are found, from Equations (3.71) and (3.72), as:

$$\ddot{y} = V_{M_O}\dot{\gamma} \tag{4.25}$$

and

$$\ddot{z} = V_{M_O}\dot{\sigma}. \tag{4.26}$$

These twenty-six equations, Equations (4.1) through (4.26), are the equations to be programmed and scaled. Before a scaled diagram can be completed, the encounters and limits on the variables must be determined. A scaling table then may be completed as the basis for the scaled diagram.

Encounter Conditions

The missile and target encounter conditions are assumed as follows:

1. The collision course encounter is a constant bearing course, preset prior to launching the

missile. Neither the target nor the missile change headings during the encounter.

2. These collision courses are in the x_1, y_1 plane, Figure 5, at various convenient positive values of the angle A.
3. The missile speed is 2500 feet per second, and the target's initial speed is 1000 feet per second.
4. A series of experiments was carried out where errors occur in one or more of the following:
    (a) Initial missile heading.
    (b) Initial target heading.
    (c) Initial relative position error.

    In the latter case, it was assumed that the target position was in error. However, the results would be the same if either or both were in error. This assumption was made to conserve potentiometers on the analog computer.
5. A series of encounters was carried out, whereby the target starts to change directions away from the initial collision course, to the advantage of the target, and continues to move away until collision occurs. This target maneuver was in three dimensions with a smooth path. For simplicity, the

target acceleration was constant throughout any one maneuver, and was varied from run-to-run, not to exceed 3g. When the target speed reached 125% of initial speed, the acceleration was ceased, and the target proceeded at the speed of 1250 feet per second.

The collision courses discussed in 1 and 2, preceding, are given in Table I.

TABLE I

COLLISION COURSE DATA

A Degrees	L Degrees	$\dot{R}_{x1}$ F.p.s.	t_c sec	Remarks
0	0	-1500	33.3	Tail chase
45	16.4	-1690	29.6	
90	23.6	-2290	21.8	
135	16.4	-3110	16.1	
180	0	-3500	14.3	Head on

Estimated Maximum of Variables for

Error Encounters

An estimate of the maximum of each computer variable

is required to properly scale the analog computer and prevent overloads from occurring. Each amplifier output must be amplitude scaled, and a rather rough, safe estimate usually is made. If needed, the problem can be rescaled based on more accurate data obtained during the experimental process. Table II is the amplitude scaling table for the initial encounters. Some variables were rescaled for the target maneuvers.

Scaled Computer Diagrams

For the initial encounters, the error encounters, the scaled equations are found from Equations (4.1) through (4.26) by using the scaled variable values of Table II. The scaled equations were programmed, resulting in a scaled computer diagram. This diagram is shown in Figures 8, 9, and 10. Each of the equations required at least one amplifier, and some required as many as five. The sequential order of Equations (4.1) through (4.26) allows rapid construction of the scaled computer diagram which, in turn, aids in the patching of the computer. Both the scaled equations and the scaled computer diagram are necessary for checking the patching of the analog computer. For example, the amplifier A03 in Figure 8 represents the scaled equation

$$2 \times 10^{-5} \rho_{MY} = -\int\{[1](p22) + \left[\frac{\dot{x}}{2500}\right](p02) - \left[\frac{\dot{y}}{2500}\right](p00)\}dt,$$

which, with potentiometer values

TABLE II

AMPLITUDE SCALING - ERROR ENCOUNTERS

Variable	Units	Estimated Maximum	Rounded-up Maximum	Scaled Variable
$\dot{u}$	fps.	1000	1000	$10^{-3}\dot{u}$
$\dot{v}$	fps.	1000	1000	$10^{-3}\dot{v}$
$\dot{w}$	fps.	1000	1000	$10^{-3}\dot{w}$
$\dot{x}$	fps.	2500	2500	$4 \times 10^{-4}\dot{x}$
$\dot{y}$	fps.	2500	2500	$4 \times 10^{-4}\dot{y}$
$\dot{z}$	fps.	2500	2500	$4 \times 10^{-4}\dot{z}$
ρ_{tx}	feet	38,000	50,000	$2 \times 10^{-5}\rho_{tx}$
ρ_{ty}	feet	50,000	50,000	$2 \times 10^{-5}\rho_{ty}$
ρ_{tz}	feet	10,000	10,000	$10^{-4}\rho_{tz}$
ρ_{Mx}	feet	100,000	100,000	$10^{-5}\rho_{Mx}$
ρ_{My}	feet	50,000	50,000	$2 \times 10^{-5}\rho_{My}$
ρ_{Mz}	feet	10,000	10,000	$10^{-4}\rho_{Mz}$
R_x	feet	50,000	50,000	$2 \times 10^{-5}R_x$
R_y	feet	8,000	10,000	$10^{-4}R_y$
R_z	feet	8,000	10,000	$10^{-4}R_z$
$\rho_{tx} + R_o$	feet	88,000	100,000	$10^{-5}(\rho_{tx} + R_o)$
$-\dot{R}_{x1}t$	fps.	50,000	50,000	$2 \times 10^{-5}[-\dot{R}_{x1}t]$
λ	rad.	1.5	2	0.5λ
δ	rad.	1.5	2	0.5δ
γ	rad.	2	2	0.5γ
σ	rad.	2	2	0.5σ
$\dot{\gamma}$	rps.	0.18	0.2	$5\dot{\gamma}$
$\dot{\sigma}$	rps.	0.18	0.2	$5\dot{\sigma}$

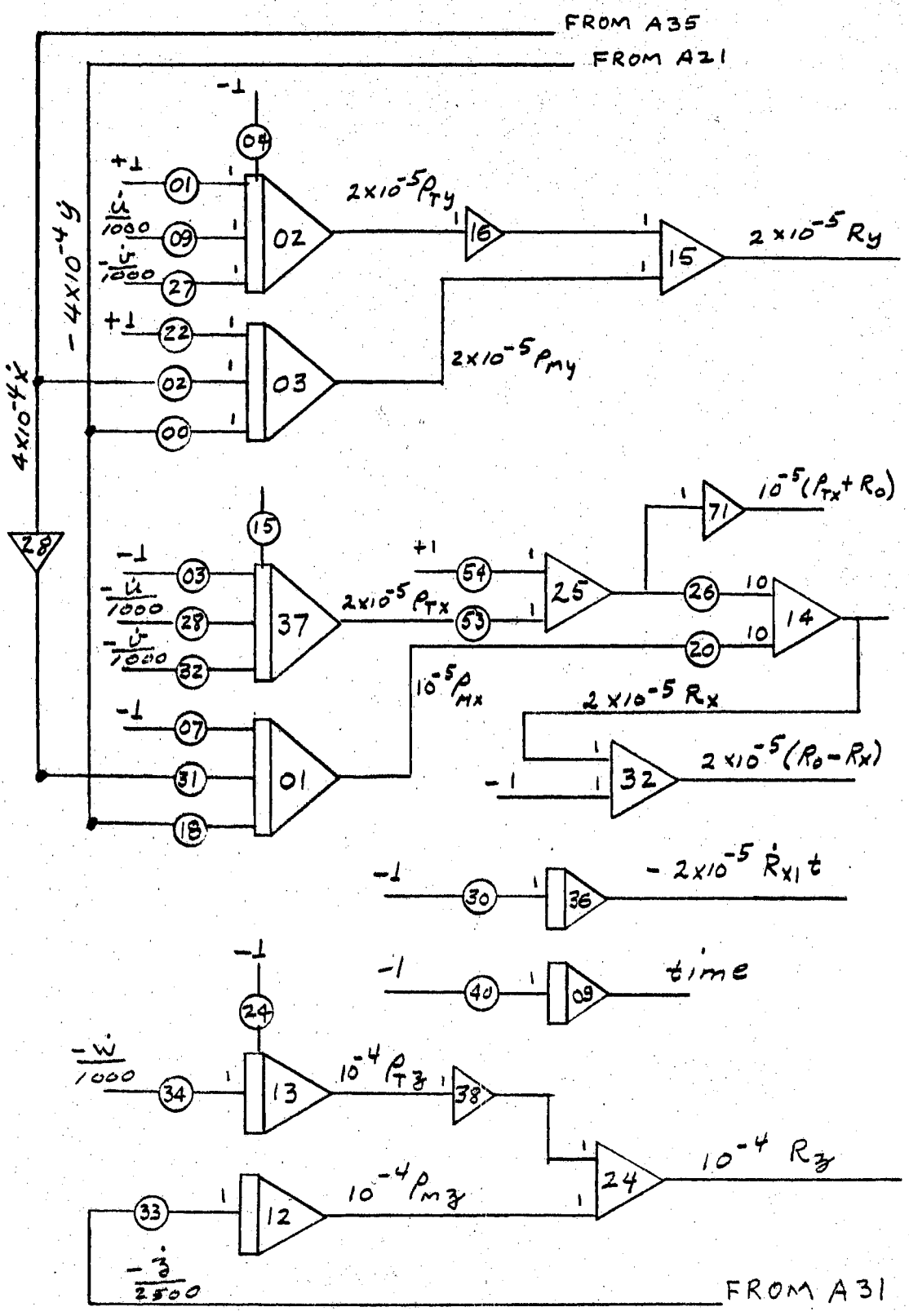

Figure 8. Scaled Computer Diagram - Error Encounter

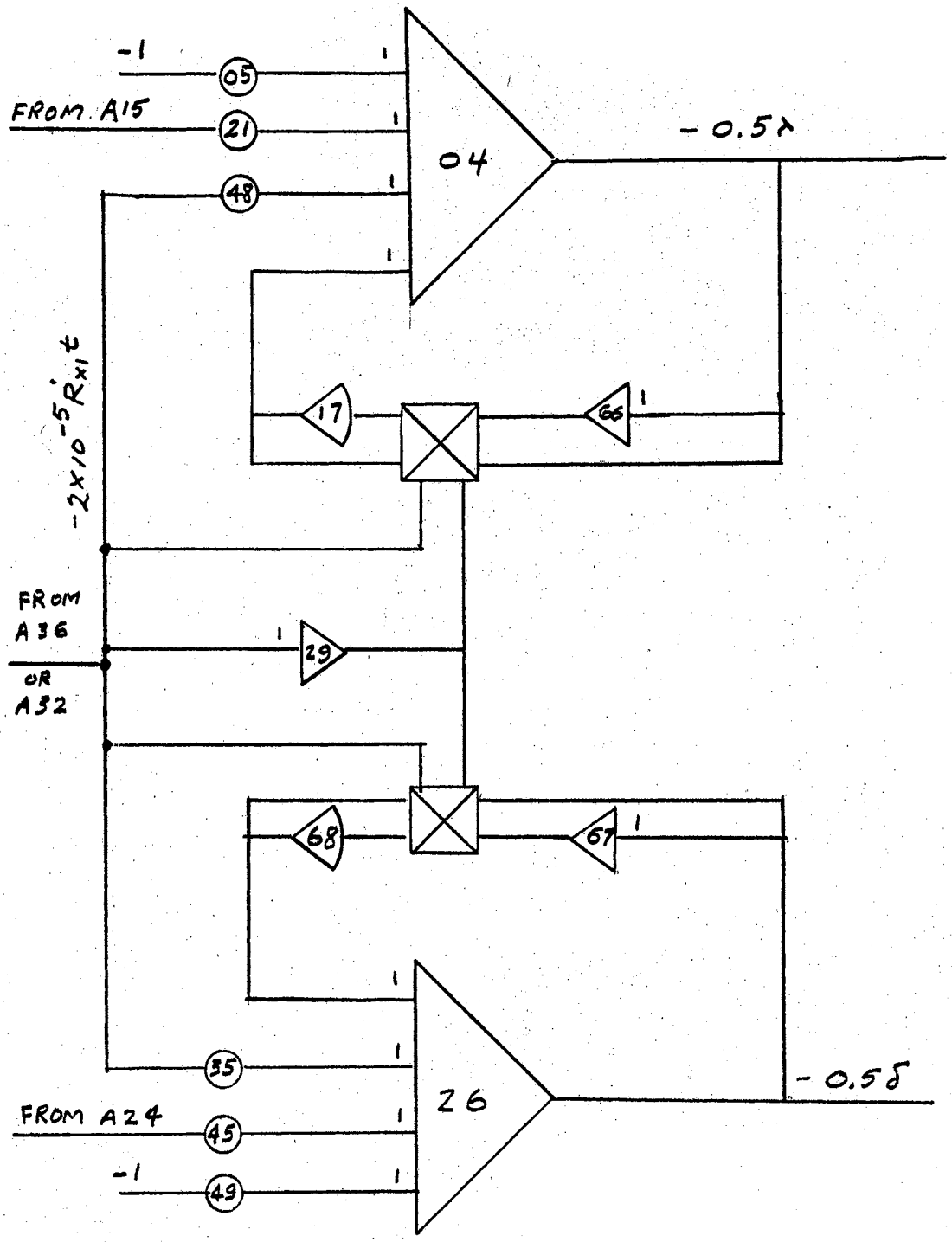

Figure 9. Scaled Computer Diagram - Error Ecnounter (Continued)

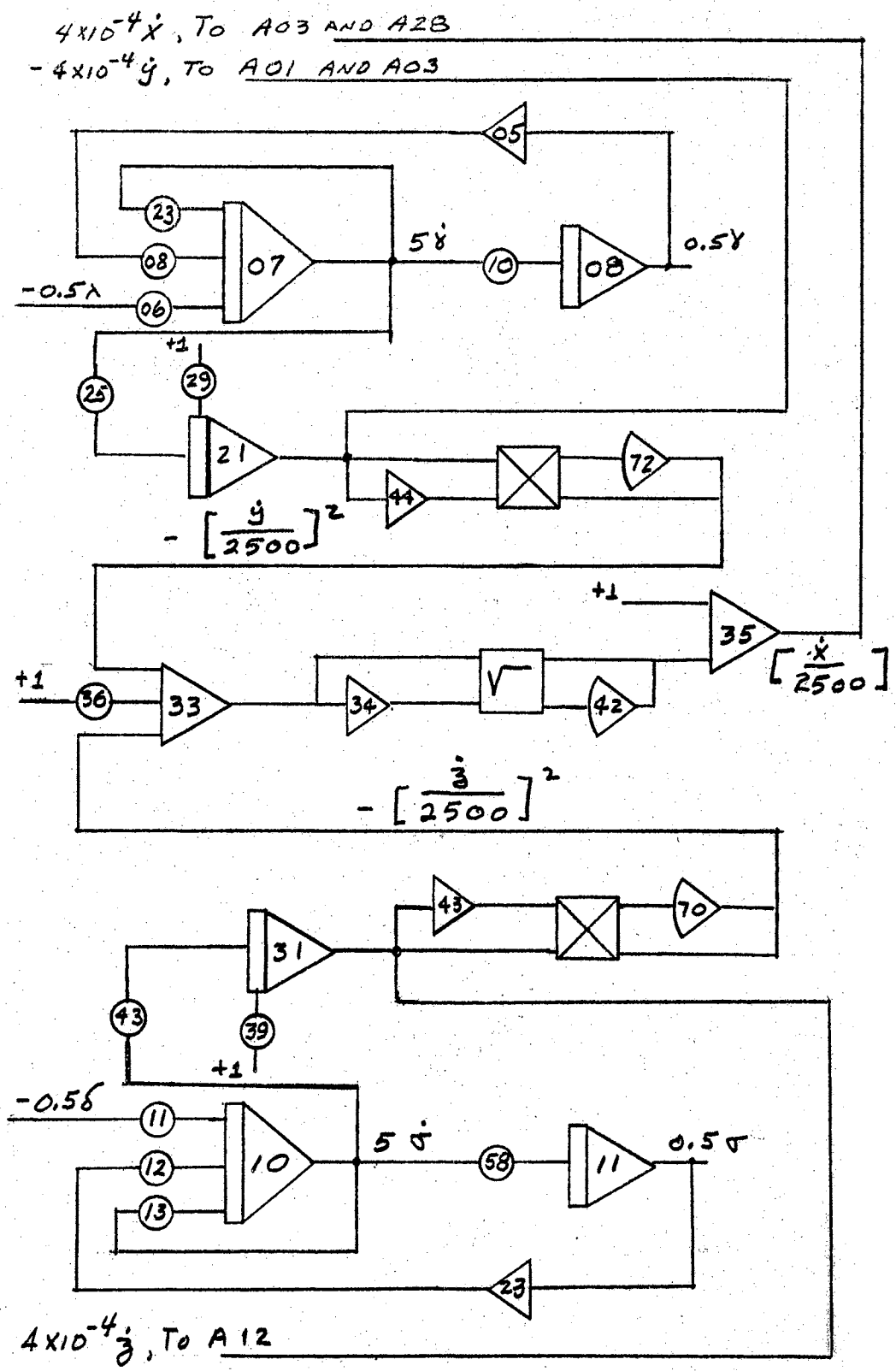

Figure 10. Scaled Computer Diagram - Error Encounter (Continued)

$$P22 = 0.05 \text{ Sin } L,$$

$$P02 = 0.05 \text{ Sin } L,$$

and $$P00 = 0.05 \text{ Cos } L,$$

reduces to Equation (4.8) when $V_{M_O} = 2500$ fps.

To simulate this system, a total of 40 amplifiers are shown in Figures 8, 9, and 10. Two additional amplifiers were used for inputs to amplifiers A04 and A26. Further, the maneuver experiments required four more amplifiers for a total of 46 amplifiers.

Target Maneuver

The target maneuver consists of modifying the foregoing equations in this chapter to accomplish Item 5 of the encounter conditions.

The unscaled equations for $\dot{u}$, $\dot{v}$, and $\dot{w}$ are found from Equations (3.45), (3.47), and (3.48), and the maneuver, as described in Item 5 of Encounter Conditions. The resultant equations are

$$\dot{u}_t = 1000 - at \quad , \quad \dot{u} = -at, \tag{4.27}$$

$$\dot{v}_t = \dot{v} = bt, \tag{4.28}$$

and

$$\dot{w}_t = \dot{w} = bt. \tag{4.29}$$

The acceleration

$$ng = \sqrt{2b^2 + a^2}\ , \tag{4.30}$$

the time for $\dot{u}_t = 0$,

$$t_1 = \frac{V_{i_0}}{a} , \tag{4.31}$$

and the 25% speed increase yield at t_1

$$V_M = \sqrt{\dot{v}^2 + \dot{w}^2} = bt_1\sqrt{2} = 1250, \tag{4.32}$$

$$a = 20.1\ n, \tag{4.33}$$

and

$$b = 0.884\ a. \tag{4.34}$$

Using these values in Equations (4.27), (4.28), and (4.29), there results the following:

$$\dot{u} = -at,$$

$$\dot{v} = 0.884\ at,$$

$$\dot{w} = 0.884\ at, \tag{4.35}$$

for $t < t_1$;

$$\dot{u} = -1000,$$

$$\dot{v} = 884,$$

and

$$\dot{w} = 884 \tag{4.36}$$

for $t_1 < t$.

These velocities will result in maximum values of

$$u = \frac{1}{n}\ (24{,}900),$$

$$v = \frac{1}{n}\ (22{,}900),$$

and

$$w = \frac{1}{n}\ (22{,}900). \tag{4.37}$$

In the target maneuver encounters, the maximum values of Table II were exceeded by some of the variables making it necessary to rescale part of the problem, using the values of those variables given in Table III. The variables not shown in Table III have the same scaled values for target maneuver as given in Table II.

TABLE III

AMPLITUDE SCALING - TARGET MANEUVER

Variable	Units	Estimated Maximum	Rounded-up Maximum	Scaled Variable
$\dot{u}$	fps.	1250	2000	$5 \times 10^{-4}\dot{u}$
$\dot{v}$	fps.	1250	2000	$5 \times 10^{-4}\dot{v}$
$\dot{w}$	fps.	1250	2000	$5 \times 10^{-4}\dot{w}$
ρ_{tz}	feet	25,000	50,000	$2 \times 10^{-5}\rho_{tz}$
ρ_{Mz}	feet	25,000	50,000	$2 \times 10^{-5}\rho_{Mz}$
R_z	feet	25,000	50,000	$2 \times 10^{-5}R_z$

The scaled computer diagram for the maneuver generator is shown in Figure 11. The output of amplifier A30 is limited to a value of 0.5 preventing the scaled variable from exceeding -5.0 volts. Thus, the velocity $\dot{u}_{max}$ = -1000 fps. Since this variable is used to generate $\dot{v}$ and $\dot{w}$,

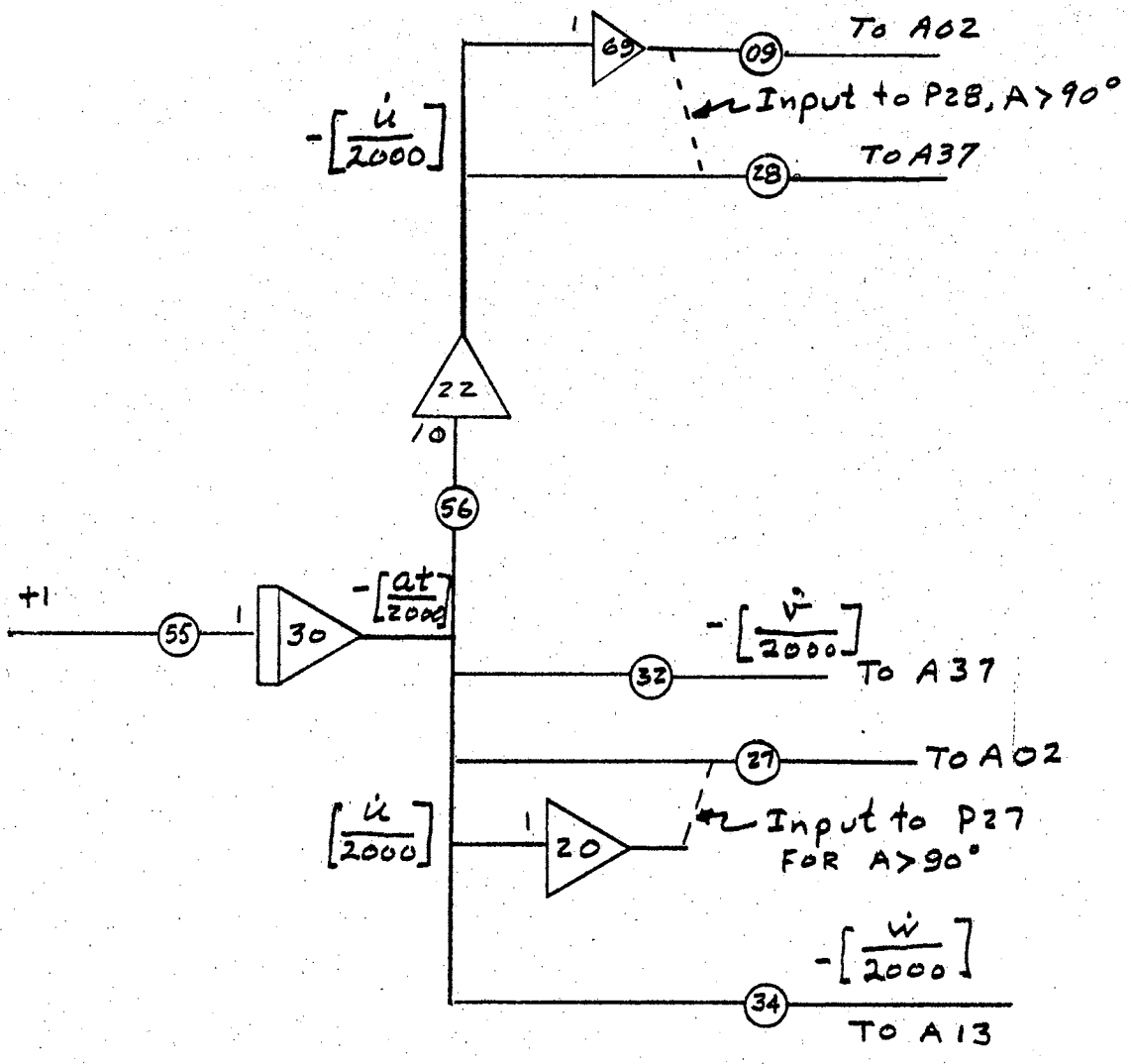

Note! Outputs of A12, A13, A38, and A24 are 0.2 times the value shown in Figure 8.

Figure 11. Scaled Computer Diagram - Maneuver Generator

they also are limited, and by proper potentiometer settings, Equations (4.35) and (4.36) are realized. Further, the limit circuits are such that this limit is not approached abruptly, which means that at time t_1 the acceleration is changing from ng to zero in a smooth manner.

The potentiometers settings and amplifier outputs are given in Appendix B for Figures 8 through 11.

CHAPTER V

ANALOG COMPUTER SIMULATION RESULTS

Introduction

The experimental results were obtained from the Electronic Analog Computer (EAI-TR-48), and plotted on rectangular grid paper using the auxiliary X - Y plotter (EAI Model 1110). The resulting plots were then analyzed.

The initial position and heading errors which were programmed for each run are given by Table IV. They consist of a calibration series of encounters, and five other series of encounters in which the target aspect angle, A, is changed from encounter-to-encounter.

The target maneuver encounter conditions are given in Table V. No heading or position errors were introduced in that encounter.

Selected traces of the results are presented in Figures 12 through 24. Tables VI, VII, and VIII present representative data in tabular form.

Calibration

The simulation calibration results are presented in Table IV, Figures 12 and 13, and in Table VI. The collision course data in Table IV, for runs 1-4, are A = 0 and

L = 0, and, for runs 5, 6, and 7, are A = 180° and L = 0. These experiments were designed to verify that the analog simulation arrangement of Figures 8, 9, and 10 does indeed operate as intended, and, further, that the analog system simulates the system described by Equations (4.1) through (4.26). Thus, these experiments are critical in determining the quality of the remaining encounters, and require further explanation as will follow.

Consider Figures 8, 9, and 10 and the various input potentiometers shown therein. If the collision course potentiometers, and those alone, are consistently set to give a particular collision course, then that course will be generated at the output of amplifiers A02, A03, A37, and A01. All other amplifiers will have voltage which result in the perturbed variables being zero. This is a trivial solution of the system of equations.

Now, consider the case where all amplifiers have an output. In general, a closed form solution representing this case is not analytically possible. However, some solutions can be found with ease. Suppose a collision course, A = 0 and L = 0, is set on the collision course potentiometers P01, P22, P03, and P07, and heading errors are set on potentiometers P09, P27, P28, P32, P29, and P39. Then, if those settings represent the velocities of calibration Run No. 1, the resulting encounter will be identical to a collision course encounter with A = 45° and L = 16.4°. All amplifiers will then have precisely that

voltage needed to trace out the curve of Figure 13a for Run No. 1, resulting in a solution of the system of equations for the initial conditions of Run No. 1.

Figure 12 shows the striking result obtained when the input potentiometers of the perturbed variables are not properly set. A curve which is not a straight line (curve B) is obtained, and, although the system amplifiers have outputs, they are not the proper values to give the predicted solution. When the mistake was rectified, curve A was obtained, producing the proper solution. This bit of serendipity vividly shows that the system yields predictable results.

Runs 2, 3, and 4 are designed to show that the system does indeed yield predictable results for other sub-systems and for other collision course solutions. The results are shown in Figure 13. Runs 5, 6, and 7 are carried out for an original collision course of A = 180° and L = 0.

The calibration encounter plots were analyzed, and the results are presented in Table VI. For all cases, the range rate $\dot{R}$ was along the range vector. Further, in all cases the resulting curves were predicted by the system of equations describing the encounter.

Missile and Target Heading and Position Errors

In Encounters I through V, errors in the collision course were introduced to determine the missile response. These errors, as shown in Table IV, were comprehensive and

selective. The initial range, as assumed, was always R_o = 50,000 feet, with errors as much as 15%, which in itself was quite a large error. The missile heading errors were as much as 11.5° with target heading errors up to 18°. The heading errors were in three dimensions for both missile and target, while the position errors were assumed to be contributed by the target and were in three dimensions.

Consider Encounter III, Run No. 11, in which A = 90° and L = 23.6°. From Table IV, it is seen that the perturbed variables are initially given maximum errors in position and headings. The results are shown in Figure 14. Figure 14(a) shows the x - y and x - z projections of the missile and target paths. The point M_o is the initial missile position, while the point T_o is the assumed location of the target at the start of mid-course guidance. The target also was assumed to be heading along -Y in the x - y plane. Figures 14(b) and (c) show the missile and target scalar components and the range components R_x, R_y, and R_z as they vary with time from the initial conditions. When the missile closes on the target to some value R_x at a time t, the value of all scalar positions can be found at that precise time from Figures 14(b) and (c). The slopes of the curves ρ_{mx}, ρ_{tx}, etc., yield the range rates. Note that the reference is along the original line of sight.

Example: At 24.5 seconds, it is found that

$$R_x = 5000 \text{ feet},$$

$$R_Y = 1500 \text{ feet},$$

$$R_Z = 800 \text{ feet},$$

$$\dot{\rho}_{MX} = 2460 \text{ fps.},$$

$$\dot{\rho}_{MY} = -340 \text{ fps.},$$

$$\dot{\rho}_{MZ} = 75 \text{ fps.},$$

$$\dot{\rho}_{tX} = -306 \text{ fps.},$$

$$\dot{\rho}_{tY} = -900 \text{ fps.},$$

and $$\dot{\rho}_{tZ} = 306 \text{ fps.}$$

These data were found from Figures 14(b) and (c), and, when analyzed, yielded the results for R and $\dot{R}$ as presented in Table VII. The results are R = 5300 feet, at direction angles 19°, 74°, and 82°, and $\dot{R}$ = 2510 fps. at direction angles 150°, 120°, and 92°. It is interesting to note that at 27 seconds the missile hits the target (R = 0).

In Figure 14(d), the perturbed missile velocity components in missile coordinates are shown. Although static checks of the analog circuit (Figure 10), which computes $\dot{x}$, were made, it is interesting to note that the dynamic values of the $\dot{x}$ calculation can be obtained from Figure 14(d). For example, at t = 20 seconds, $\dot{y}$ = 695 fps, $\dot{z}$ = 75 fps, and $\dot{x}$ = -100 fps, from Equation (4.23) $\dot{x}$ is found as follows:

$$\dot{x} = -2500 + \{(2500)^2 - (695)^2 - (75)^2\}^{\frac{1}{2}}$$

$$\dot{x} = -2500 + 2402 = -98 \text{ fps.}$$

Other points yield similar results, giving further

credence to that particular part of the analog simulation.

Other error encounters are illustrated by Figures 15 and 16. The resulting ranges and range rates for those and other runs are given by Table VII. Figure 15 shows Encounter IV, Run No. 3, in which extreme missile turns are made. Figure 16 shows two different head-on encounters.

Target Maneuver

The results of the target maneuver encounters are presented in Tables V and VIII and in Figures 17 through 24. Table V contains the initial collision course target acceleration and final target attitude for each run. Further, the variable used in calculating the rate of change of the line of sight is indicated by the appropriate mark in the columns for R_1 or for R_x.

While these experiments were being carried out, it became apparent that unrealistic oscillations occurred in the missile path due to the line of sight calculation using R_1. Equations (3.75) through (3.78) represent a revision in the analog system in which R_x is used instead of R_1.

The effectiveness in using R_x is seen by comparing Runs 2b and 2e in Figures 17 and 18, and by comparing Runs 2c and 2d in Figures 19 and 20. In Runs 2b and 2c, R_1 was used, while in Runs 2d and 2e, R_x was used. In each case, less oscillation occurred when R_x was used. Perhaps the most vivid example is shown in Figures 21 and 22 in which

a 3g maneuver is made by the target. Oscillations occur in Figure 21 for Run 3c, which uses R_1. These oscillations start at $R_1 = 0$, and occur thereafter, missing rather badly. In Figure 22, Run 3d is identical to Run 3c except for use of R_x instead of R_1, and the missile path is much improved over Figure 21.

Figures 23 and 24 are other encounters using R_x, and were also improvements over the same encounters using R_1.

General Results

The results presented in Tables VI, VII, and VIII describe the range vector and range rate vector for some selected runs. When all of the encounters are considered, assuming mid-course guidance ends at $R_x = 5000$ feet, the missile appears to be controllable by the terminal guidance phase to within a reasonable miss distance of the target. Even when the terminal guidance phase is not considered, assuming that the mid-course guidance operates all the way until $R_x = 0$, the results are most favorable.

As a measure of quality, the results of each run were examined at $R_x = 0$ as if there were no terminal guidance. The results are as follows:

1. Encounters 56 ;
2. Direct Hits 22 ;
3. Miss, 0 to 500 ft. 15 ;
4. Miss, 500 to 1000 ft. 9 ;
5. Miss, 1000 to 2000 ft. 4 ;

6. Miss, 2000 to 5000 ft. 6 .

Of those 19 runs missing by 500 ft. or more, four were programming mistakes in Encounter III, which were later rectified, and the remaining 15 were due to $R_1 = 0$, prior to terminal conditions. This last observation was verified by Runs 2d, 2e, 3d, and 4c in which the miss distance was reduced below 500 feet, in each case, while identical runs using R_1 missed more than 500 feet.

TABLE IV

INITIAL POSITION AND HEADING ERRORS

Encounter	Run No.	Initial Value of the Variable							
		u feet	v feet	w feet	$\dot{u}$ fps.	$\dot{v}$ fps.	$\dot{w}$ fps.	$\dot{y}$ fps.	$\dot{z}$ fps.
Calibration	1	0	0	0	-293	-707	0	-707	0
	2	0	0	0	-293	0	707	0	707
	3	0	0	0	-1000	1000	0	1000	0
	4	0	0	0	-1000	0	-1000	0	-1000
	5	0	0	0	-1000	1000	0	1000	0
	6	0	0	0	-293	0	-707	0	-707
	7	0	0	0	-293	707	0	707	0
I (A=0)	1	0	0	0	0	0	0	500	500
	2	0	0	0	-100	200	200	500	500
	3	5,000	5,000	5,000	-100	200	200	500	500
	4	5,000	5,000	5,000	0	0	0	500	500
	5	5,000	5,000	5,000	0	0	0	0	0
	6	5,000	5,000	5,000	-100	200	200	-500	-500

TABLE IV (Continued)

Encounter	Run No.	Initial Value of the Variable							
		u feet	v feet	w feet	$\dot{u}$ fps.	$\dot{v}$ fps.	$\dot{w}$ fps.	$\dot{y}$ fps.	$\dot{z}$ fps.
	7	0	0	0	-100	200	300	0	0
II (A=45°)	1	0	0	0	0	0	0	500	500
	2	0	0	0	-100	200	200	500	500
	3	5,000	5,000	5,000	-100	200	200	500	500
	4	5,000	5,000	5,000	0	0	0	500	-500
	5	5,000	5,000	5,000	0	0	0	-500	-500
	6	5,000	5,000	5,000	-100	200	200	0	0
III (A=90°)	1	-5,000	0	0	0	0	0	0	0
	2	0	0	5,000	0	0	0	0	0
	3	-5,000	0	0	0	0	0	500	0
	4	-5,000	5,000	5,000	-100	0	0	0	0
	6	-5,000	5,000	5,000	-100	200	200	0	0
	7	-2,000	2,000	2,000	-100	100	100	0	0
	8	0	0	5,000	0	0	0	0	0

TABLE IV (Continued)

Encounter	Run No.	Initial Value of the Variable							
		u feet	v feet	w feet	$\dot{u}$ fps.	$\dot{v}$ fps.	$\dot{w}$ fps.	$\dot{y}$ fps.	$\dot{z}$ fps.
	9	-5,000	0	0	0	0	0	500	0
	10	-5,000	5,000	5,000	-100	200	200	0	0
	11	-5,000	5,000	5,000	-100	306	-306	-500	-500
	12	5,000	5,000	5,000	0	0	0	0	0
IV (A=135°)	1	0	0	0	0	0	0	500	500
	2	0	0	0	-100	200	200	-500	500
	3	5,000	5,000	5,000	-100	200	200	500	500
	4	5,000	5,000	5,000	0	0	0	-500	-500
	5	5,000	5,000	5,000	0	0	0	0	0
	6	-5,000	-5,000	5,000	0	0	0	0	0
	7	-5,000	-5,000	5,000	0	0	0	500	500
V (A=180°)	1	0	0	0	0	0	0	500	500
	2	5,000	-5,000	5,000	0	0	0	500	-500

TABLE IV (Continued)

Encounter	Run No.	Initial Value of the Variable							
		u feet	v feet	w feet	$\dot{u}$ fps.	$\dot{v}$ fps.	$\dot{w}$ fps.	$\dot{y}$ fps.	$\dot{z}$ fps.
	3	5,000	-5,000	5,000	-100	200	200	-500	-500
	4	5,000	-5,000	5,000	-100	200	200	0	0
	5	5,000	-5,000	5,000	0	0	0	0	0

TABLE V

TARGET MANEUVER ENCOUNTER CONDITIONS

Run No.	Collision Course		Target Acceleration in g's	Final Target Angle Degrees	Line of Sight Calculated Using	
	A-Degrees	L-Degrees			R_1	R_x
1a	0	0	1	-90	x	
1b	0	0	2	-90	x	
1c	0	0	3	-90	x	
2a	45	16.4	1	-45	x	
2b	45	16.4	2	-45	x	
2c	45	16.4	3	-45	x	
2d	45	16.4	3	-45		x
2e	45	16.4	2	-45		x
3a	90	23.6	1	0	x	
3b	90	23.6	2	0	x	
3c	90	23.6	3	0	x	
3d	90	23.6	3	0		x
4a	135	16.4	1	45	x	
4b	135	16.4	3	45	x	
4c	135	16.4	3	45		x
5a	180	0	3	90		x

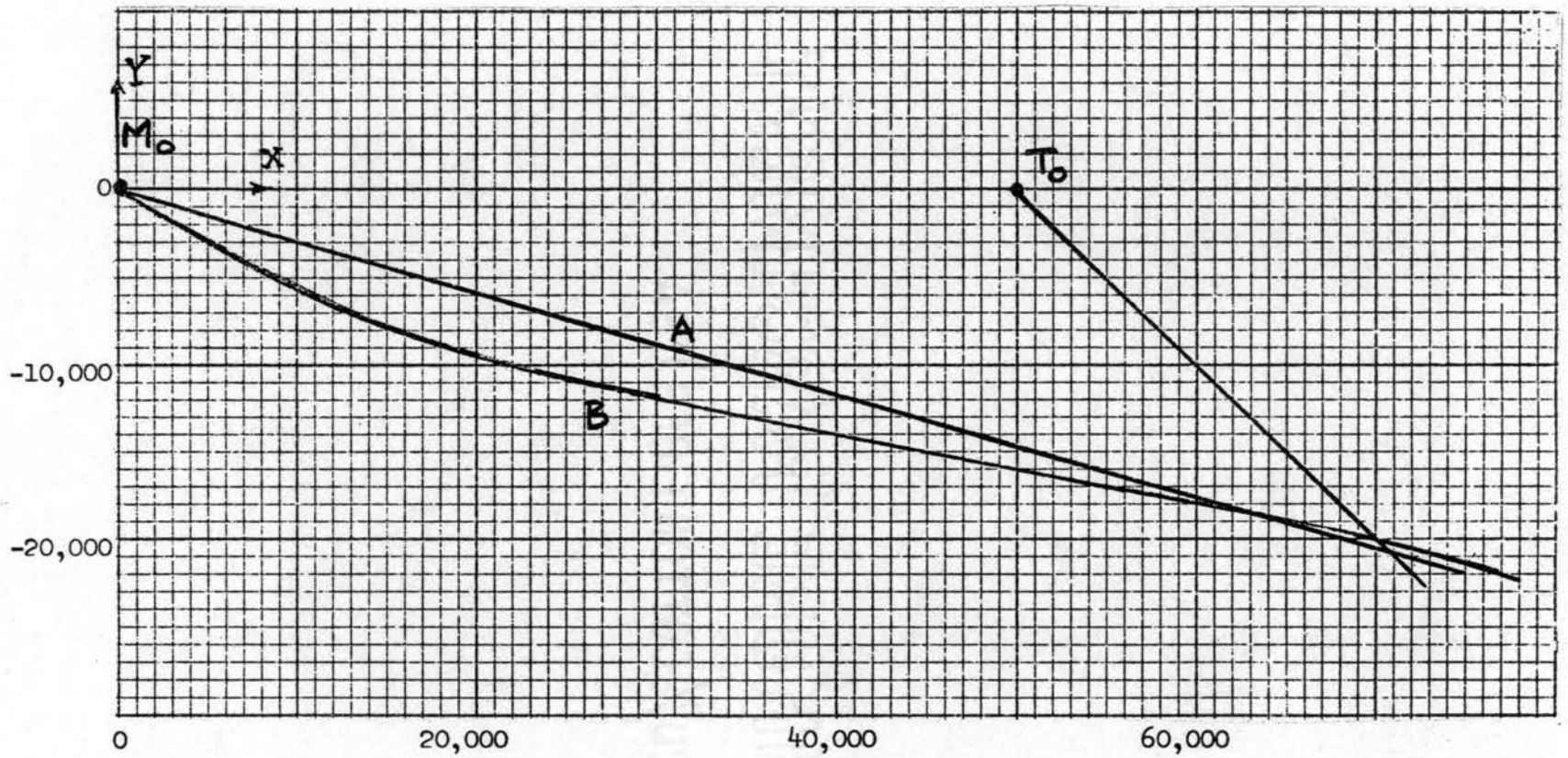

Figure 12. Calibration of Simulation System

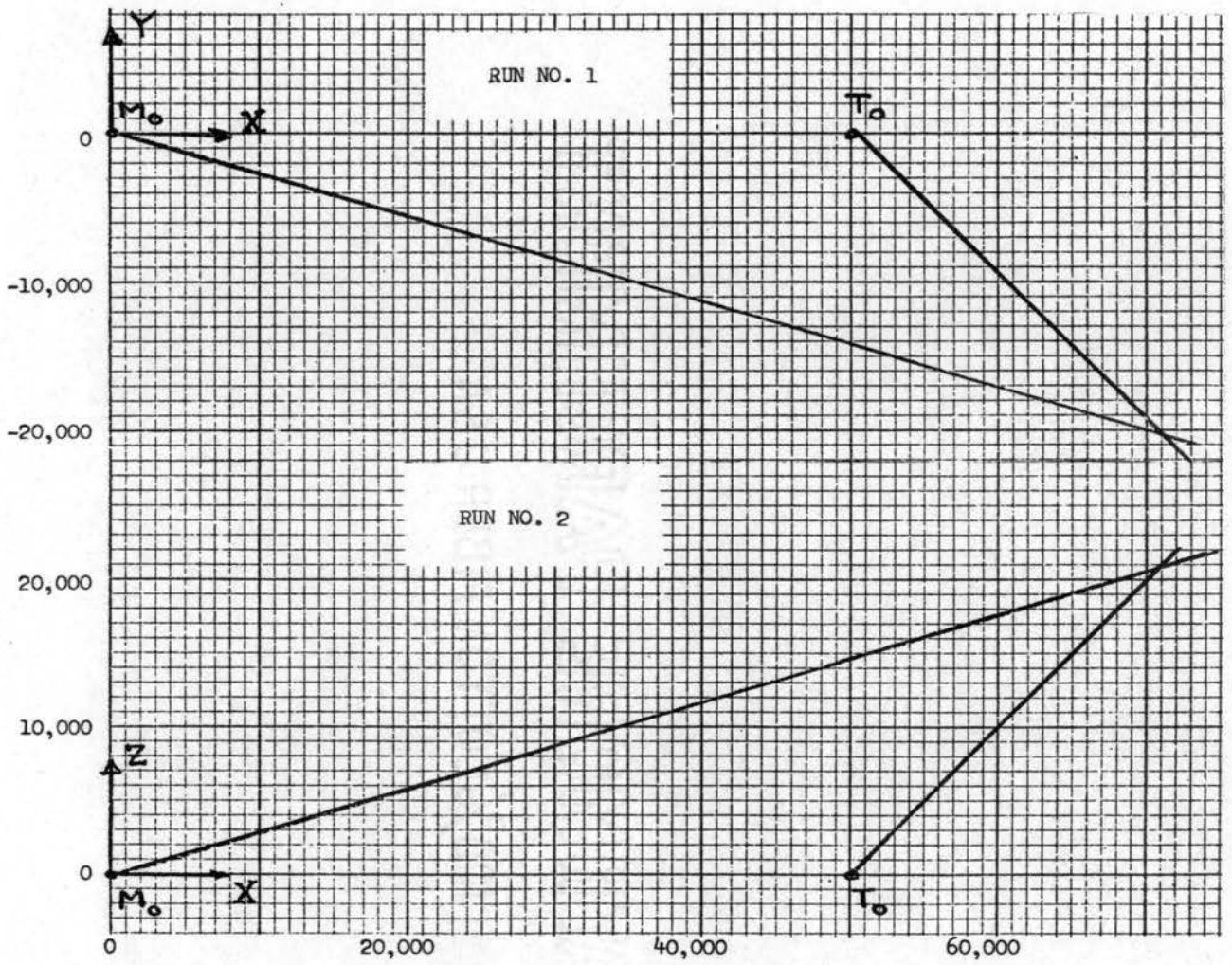

(a)

Figure 13. Calibration

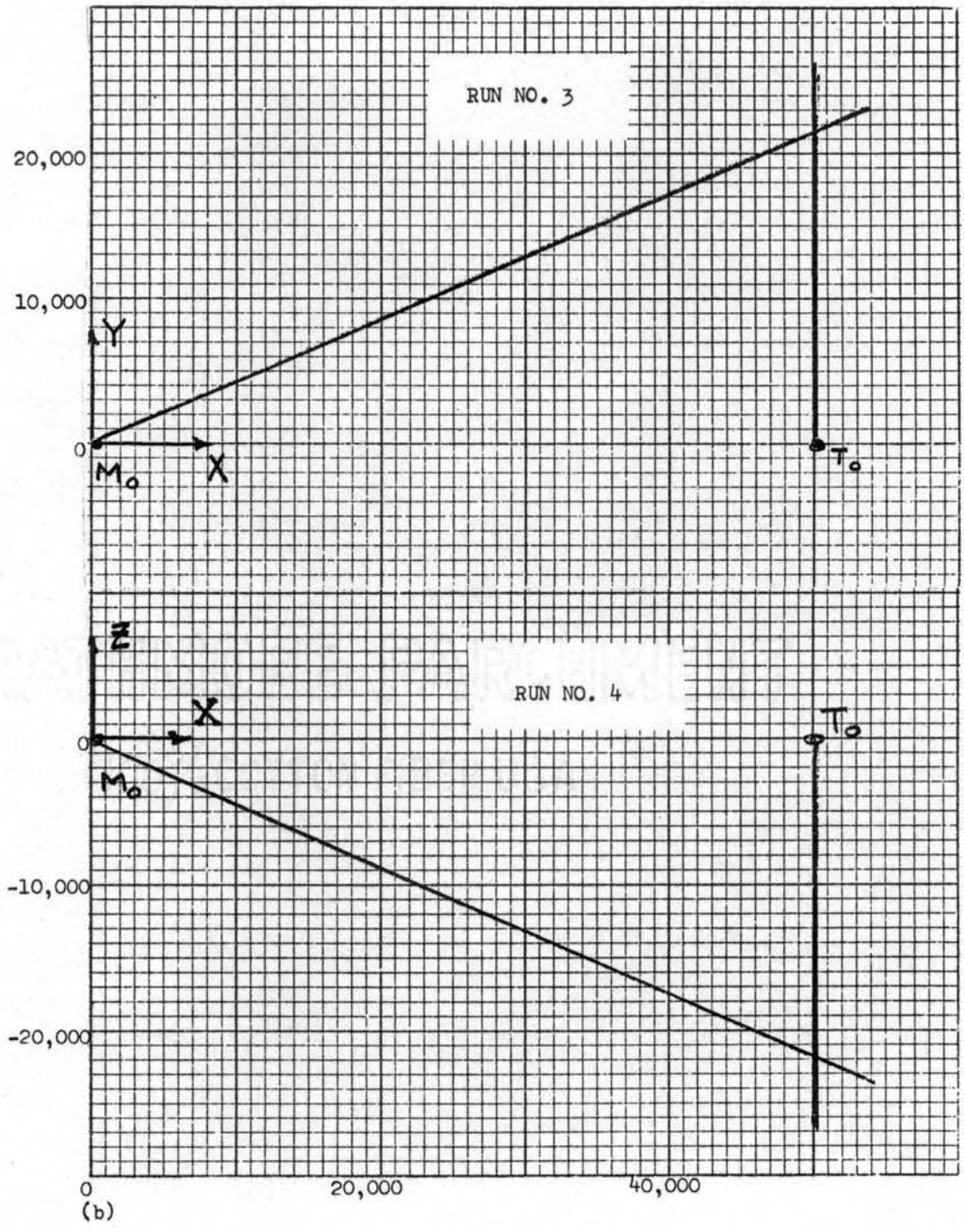

Figure 13. (Continued)

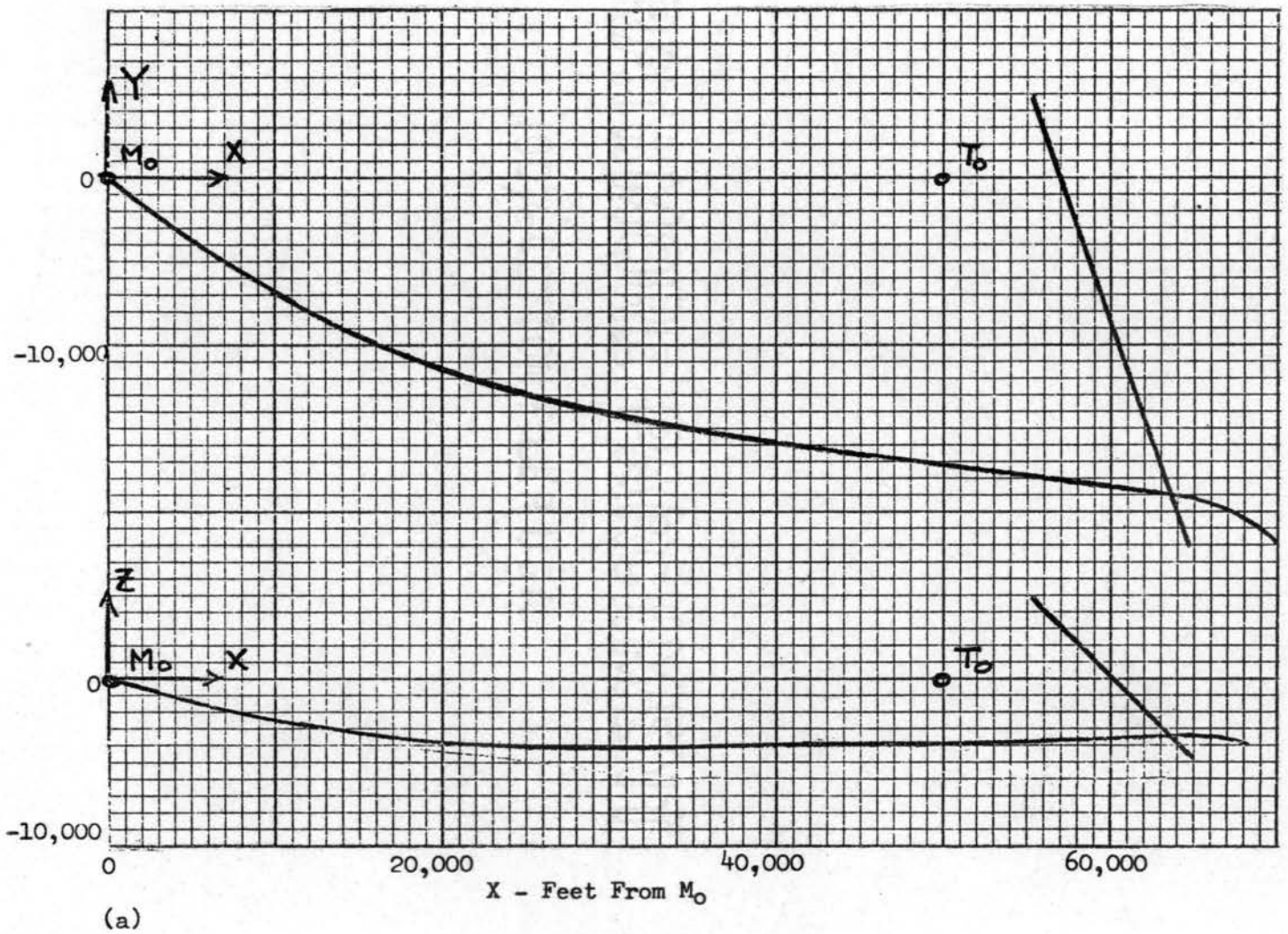

Figure 14. Encounter III, Run 11

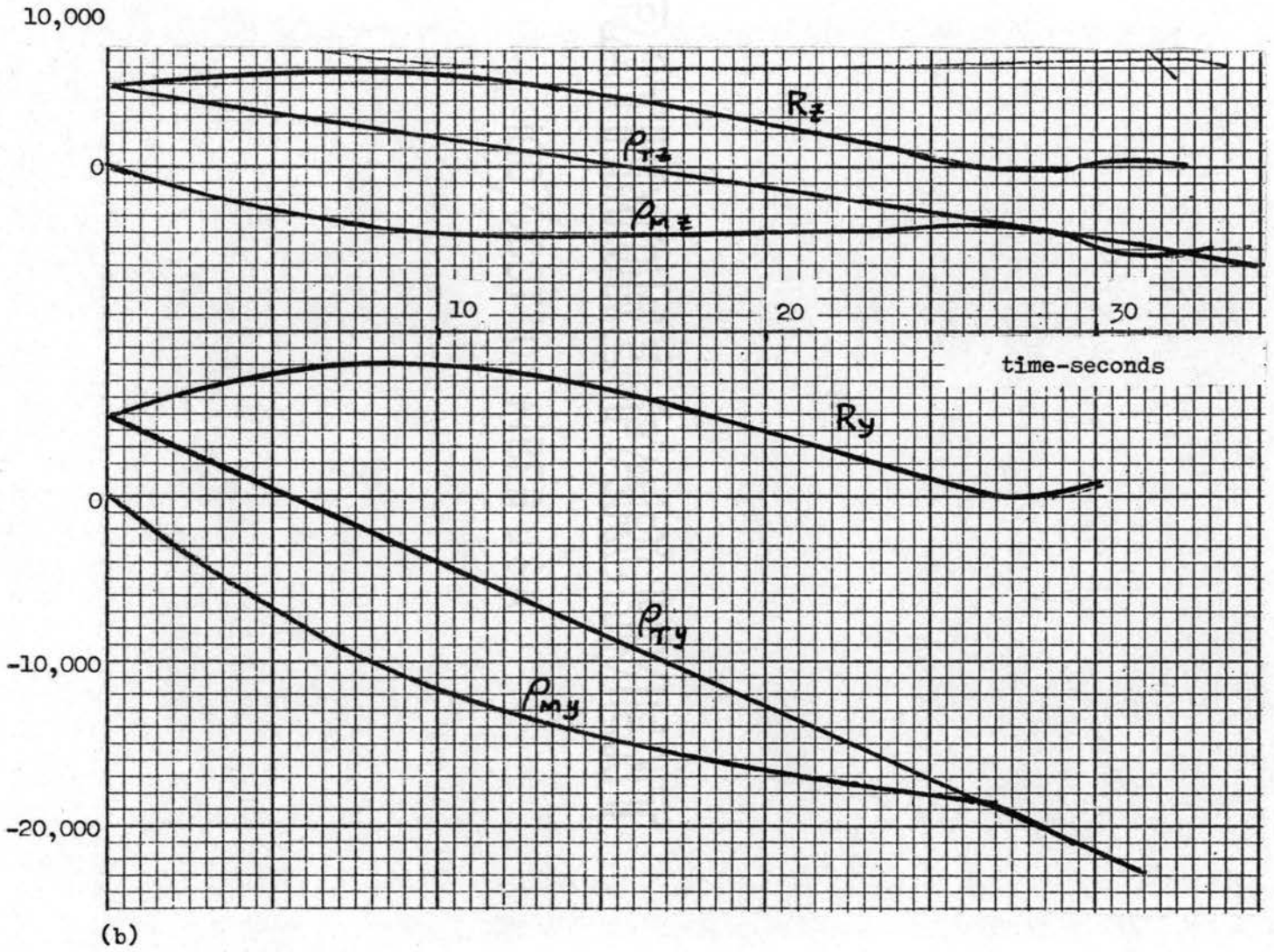

Figure 14. (Continued)

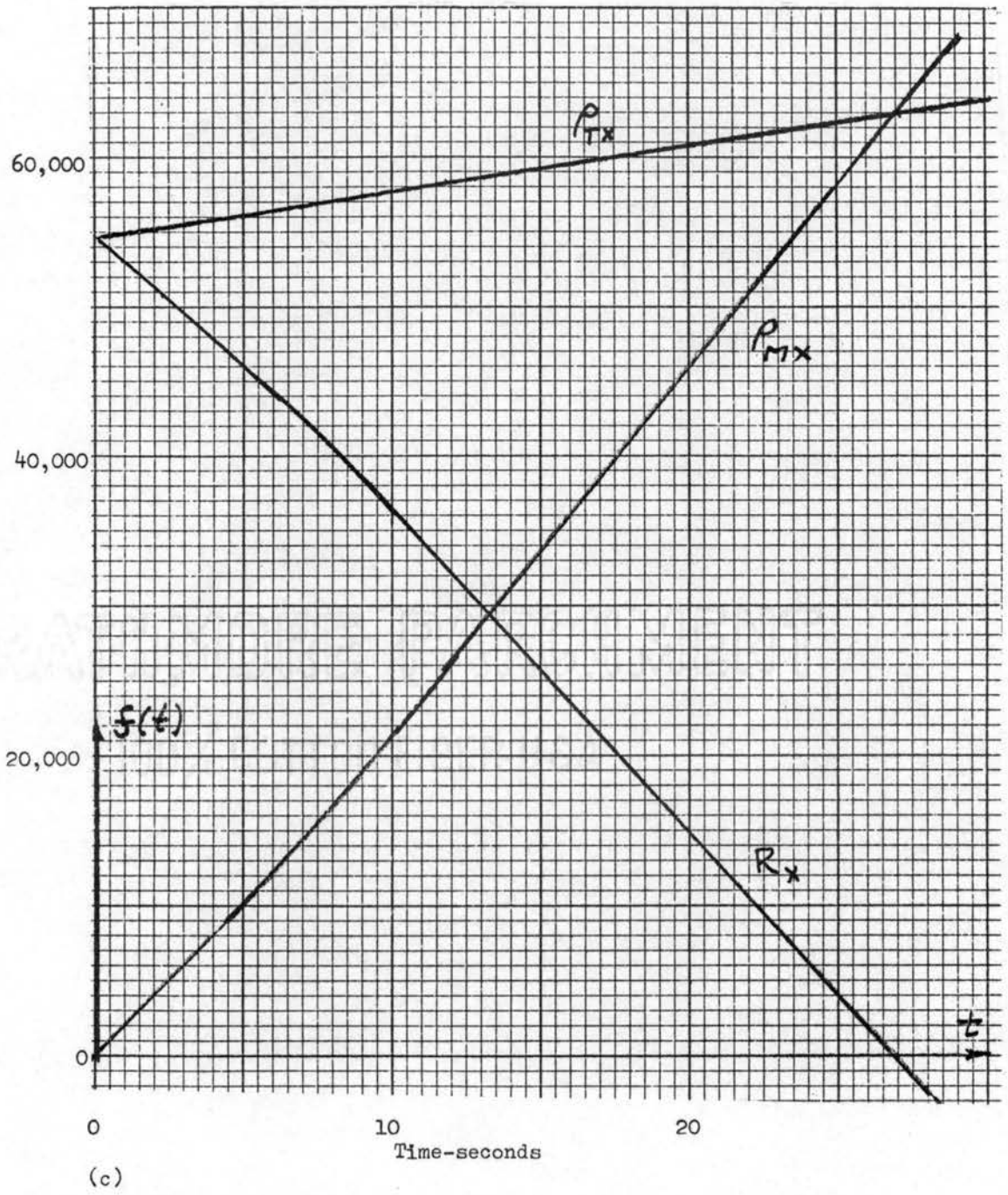

(c)

Figure 14. (Continued)

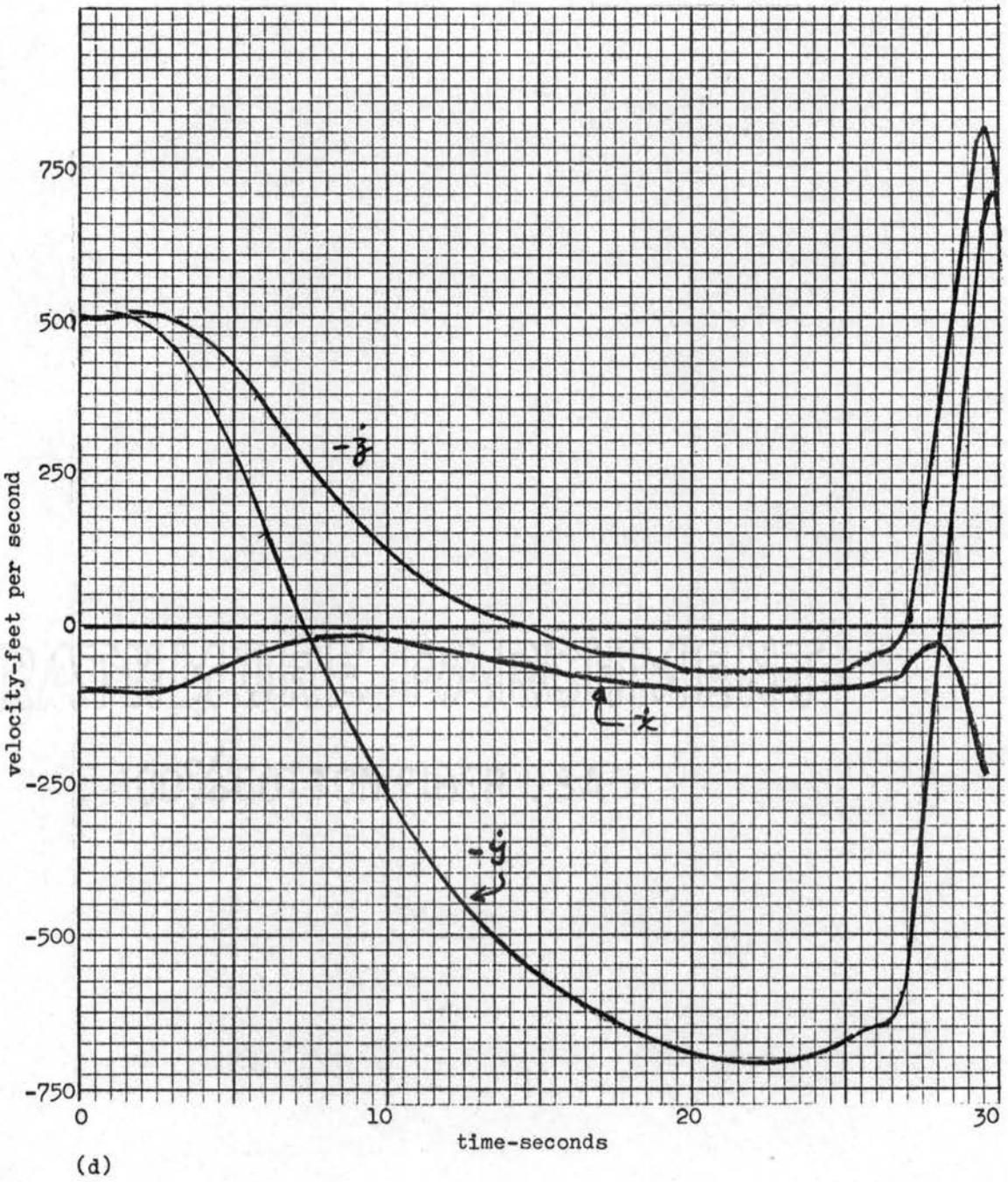

Figure 14. (Continued)

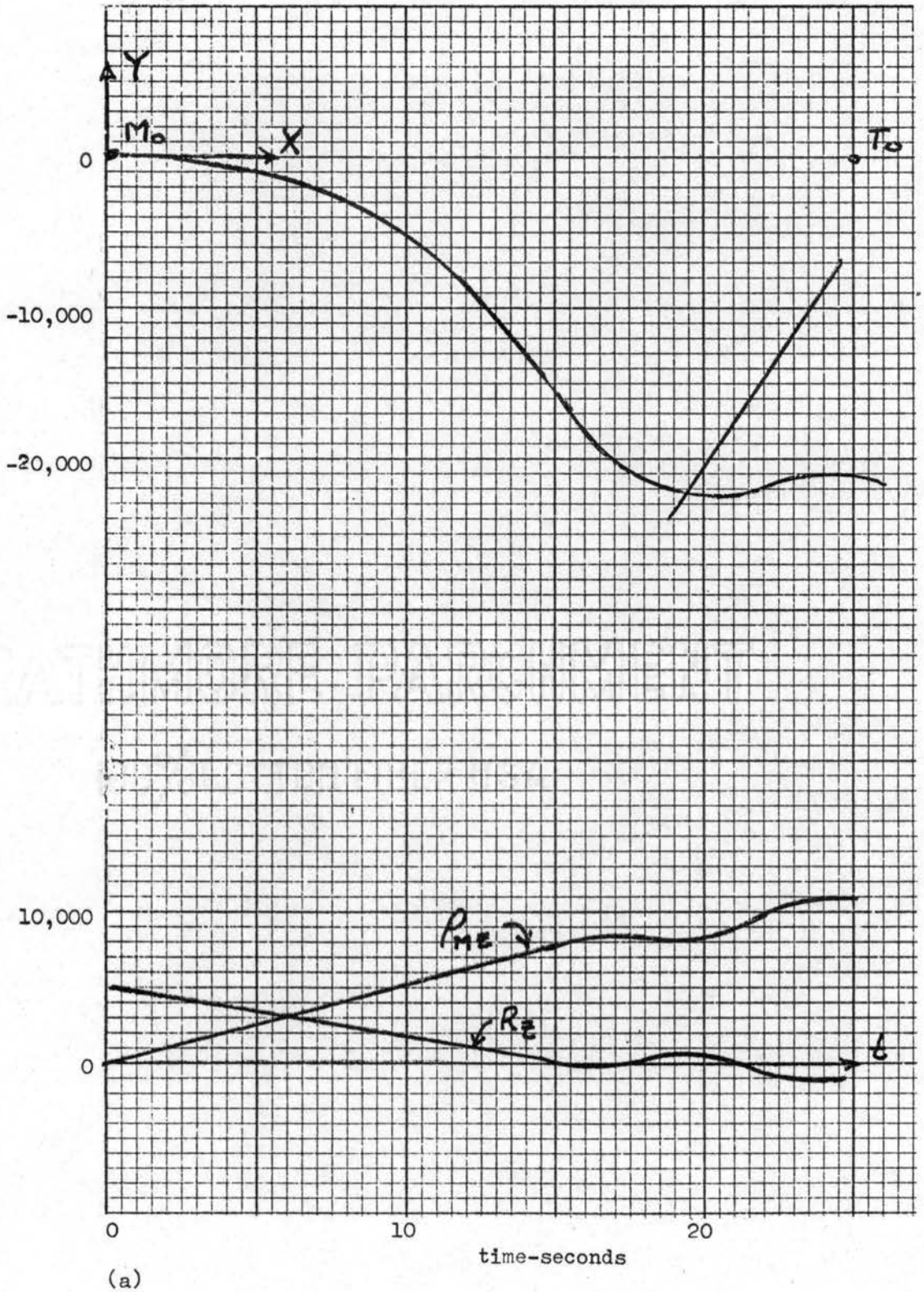

Figure 15. Encounter IV, Run 3

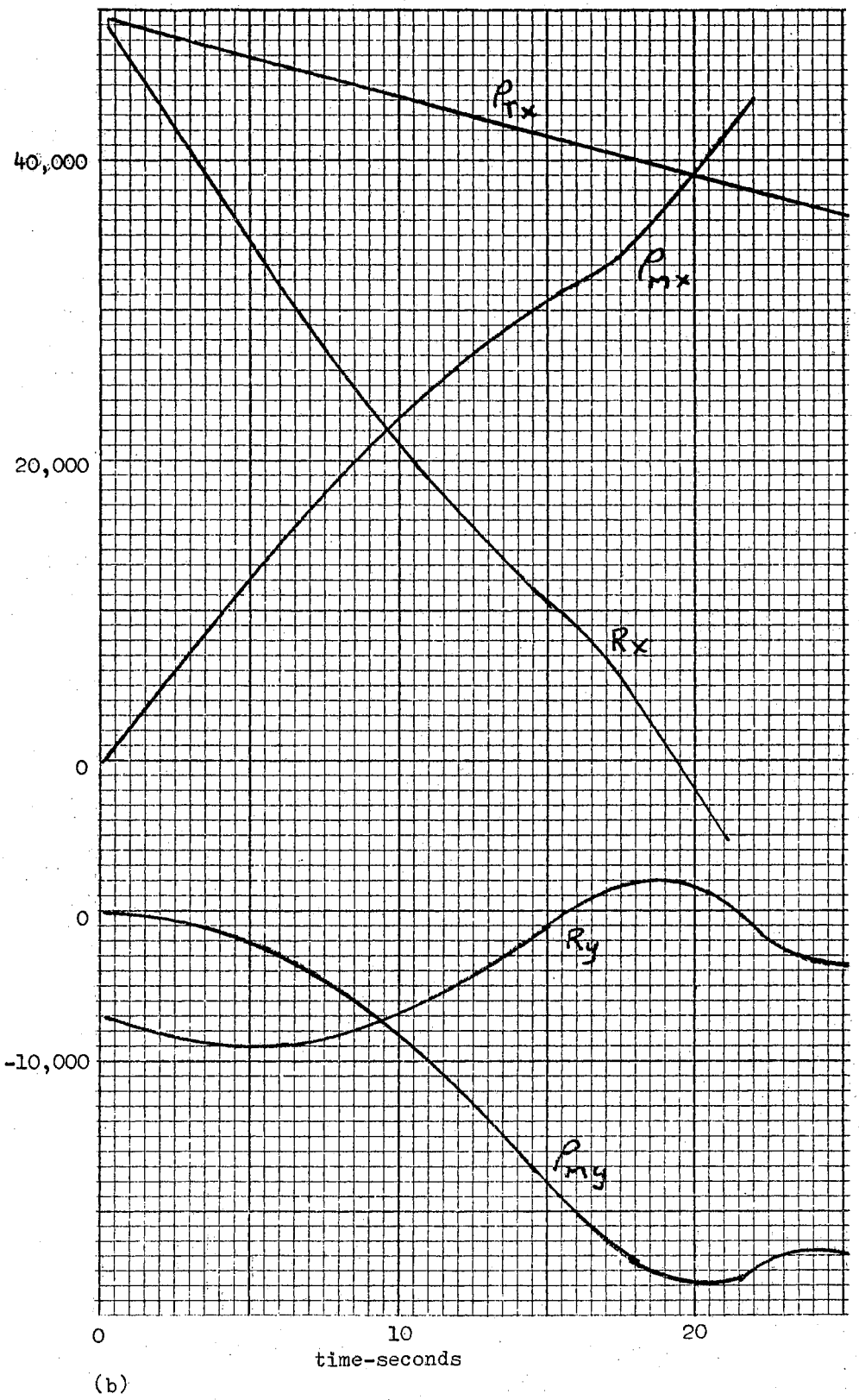

Figure 15. (Continued)

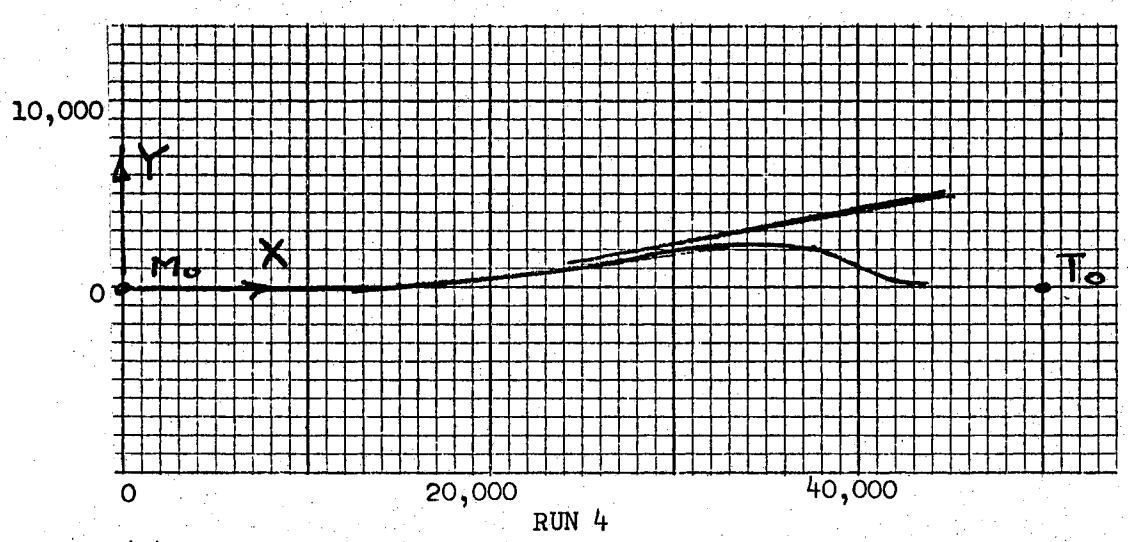

(a)

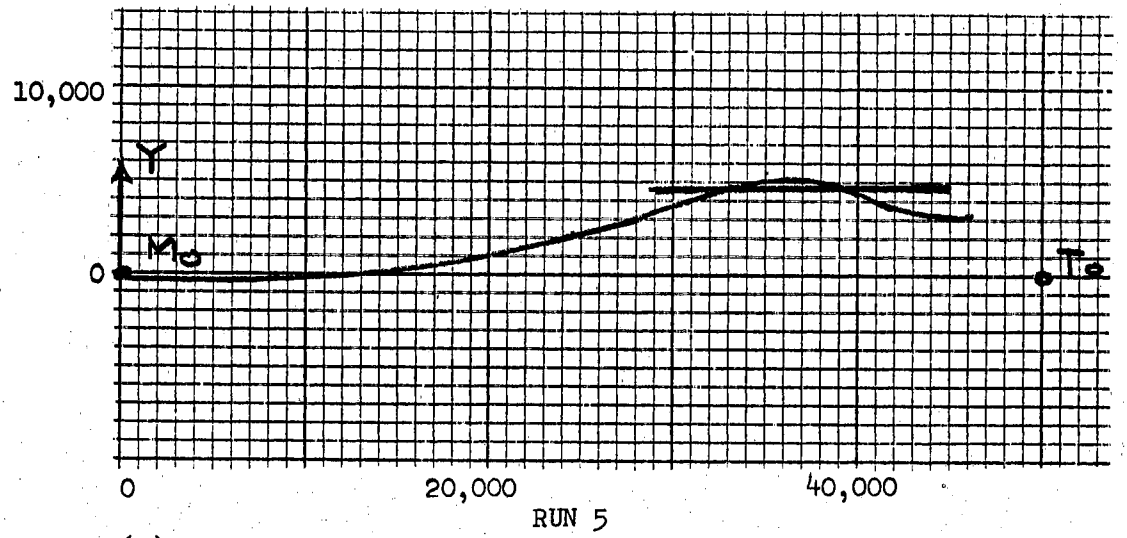

(b)

Figure 16. Encounter V, Runs 4 and 5

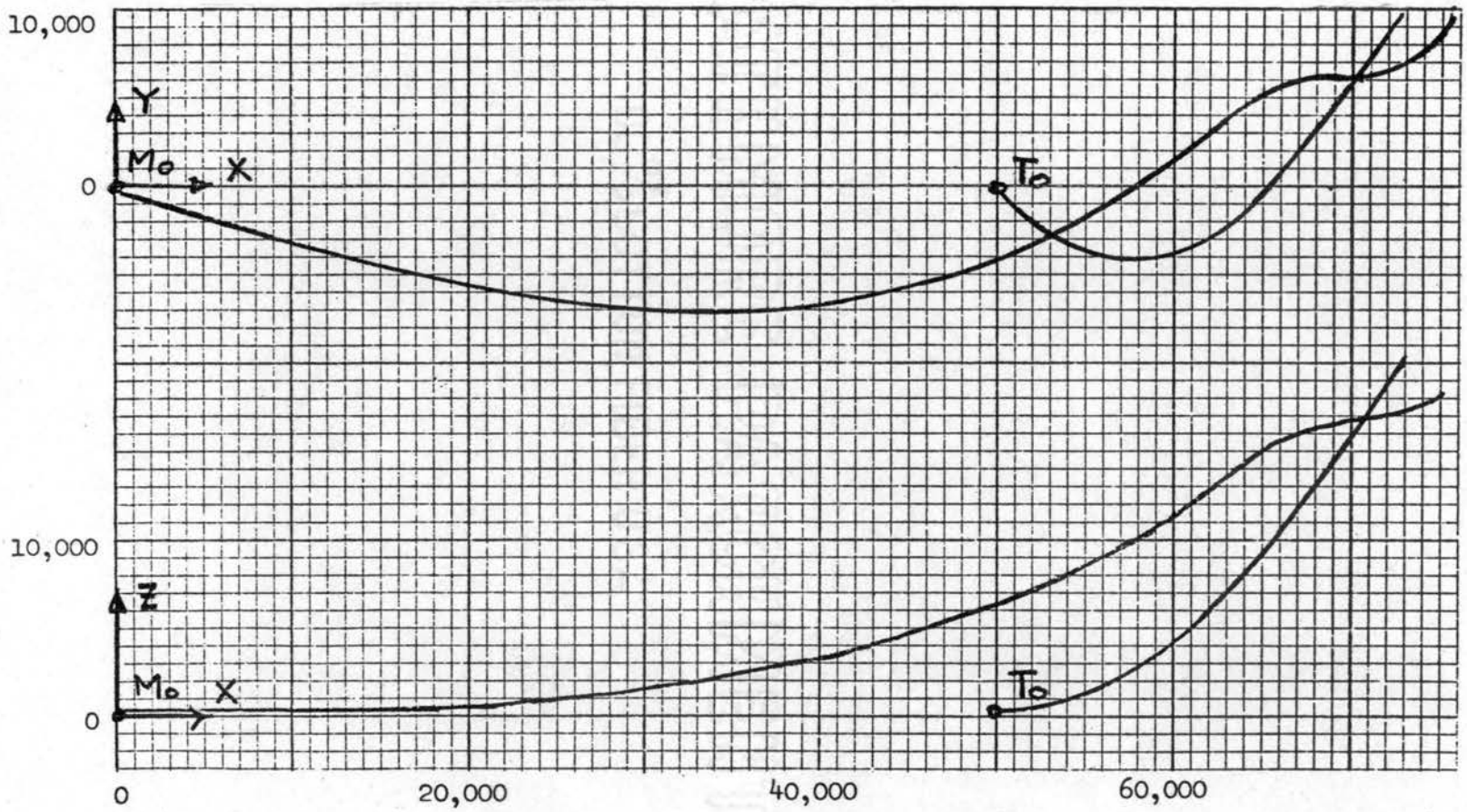

Figure 17. Encounter VI, Run 2b

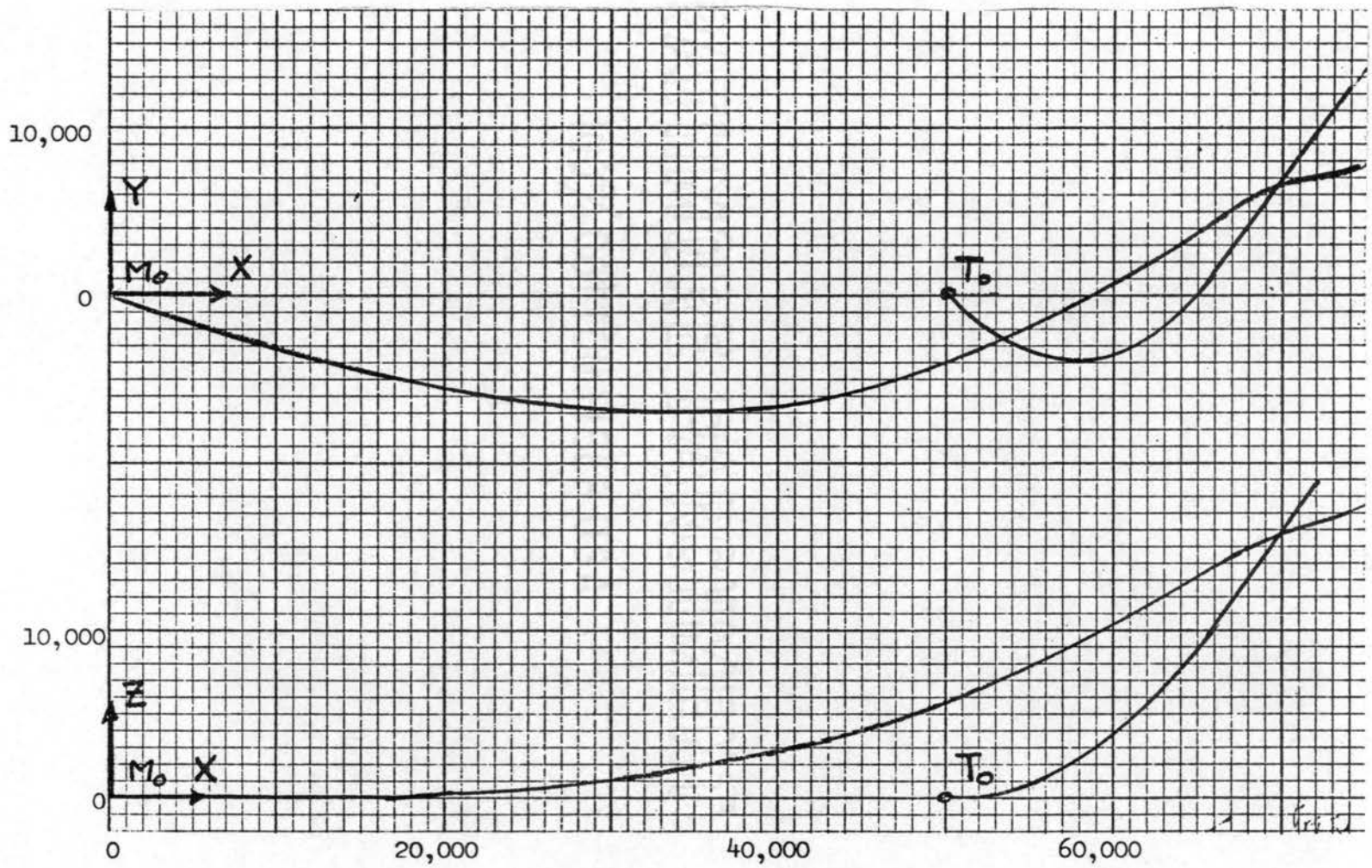

Figure 18. Encounter VI, Run 2e

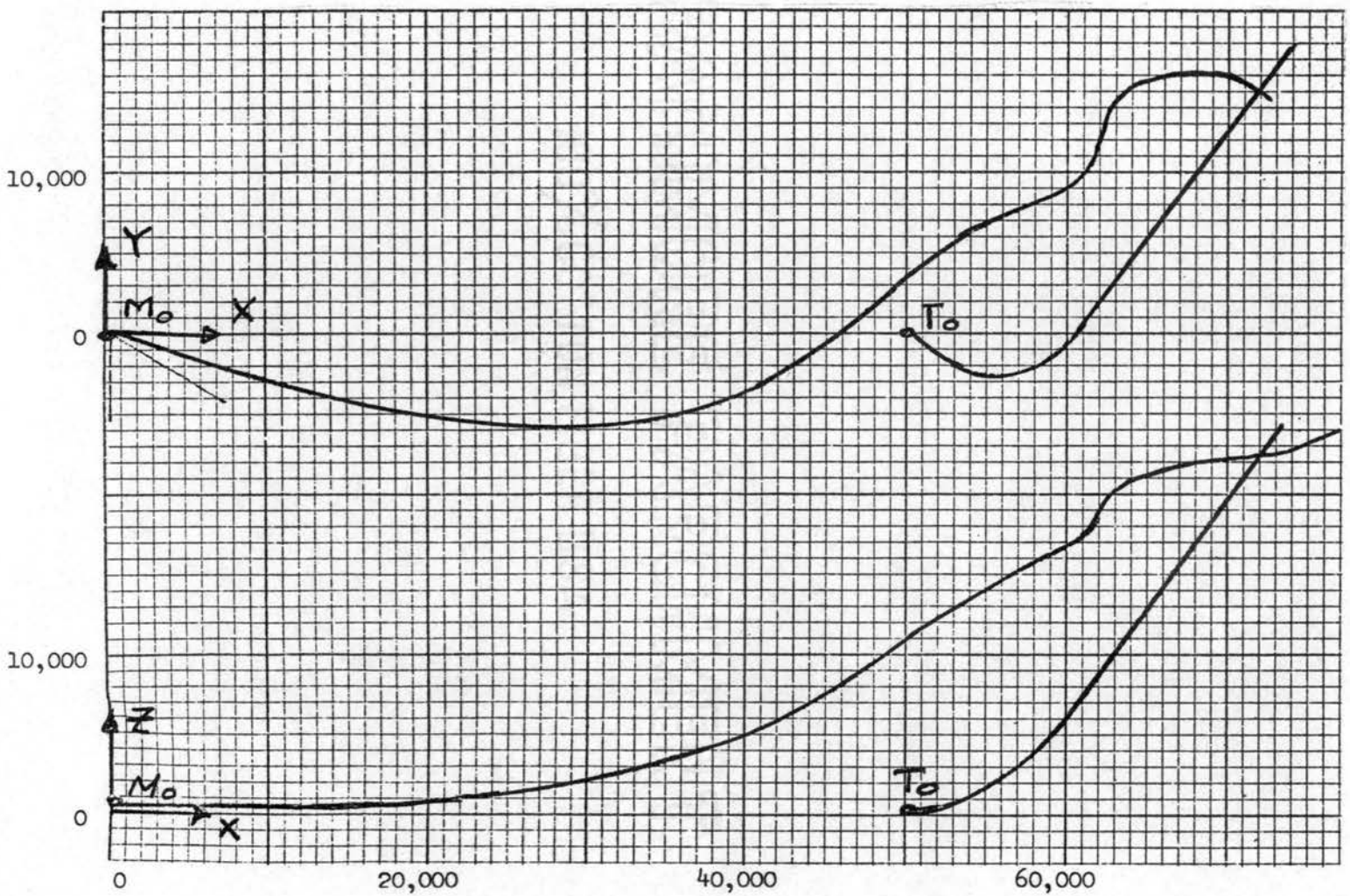

Figure 19. Encounter VI, Run 2c

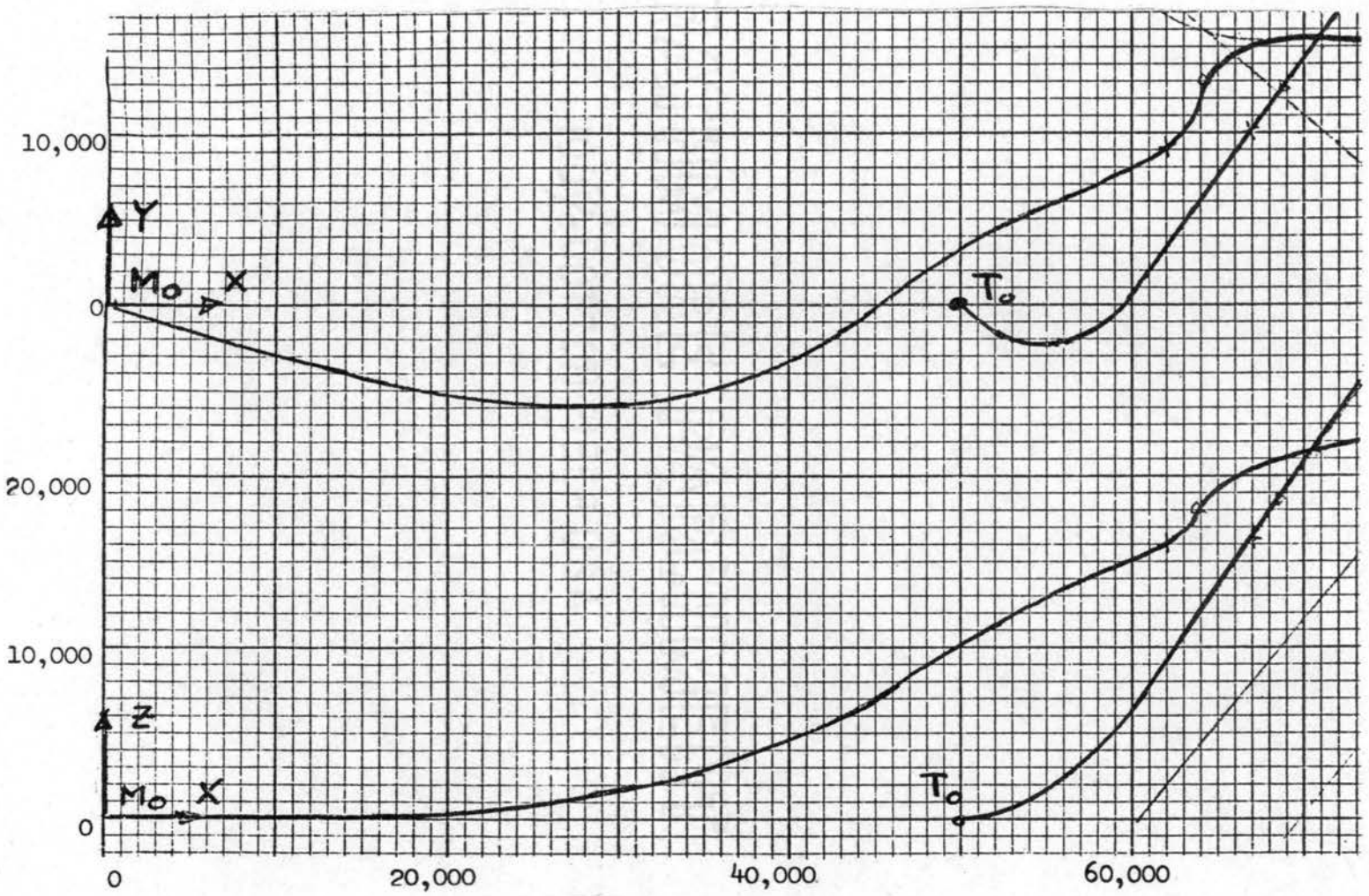

Figure 20. Encounter VI, Run 2d

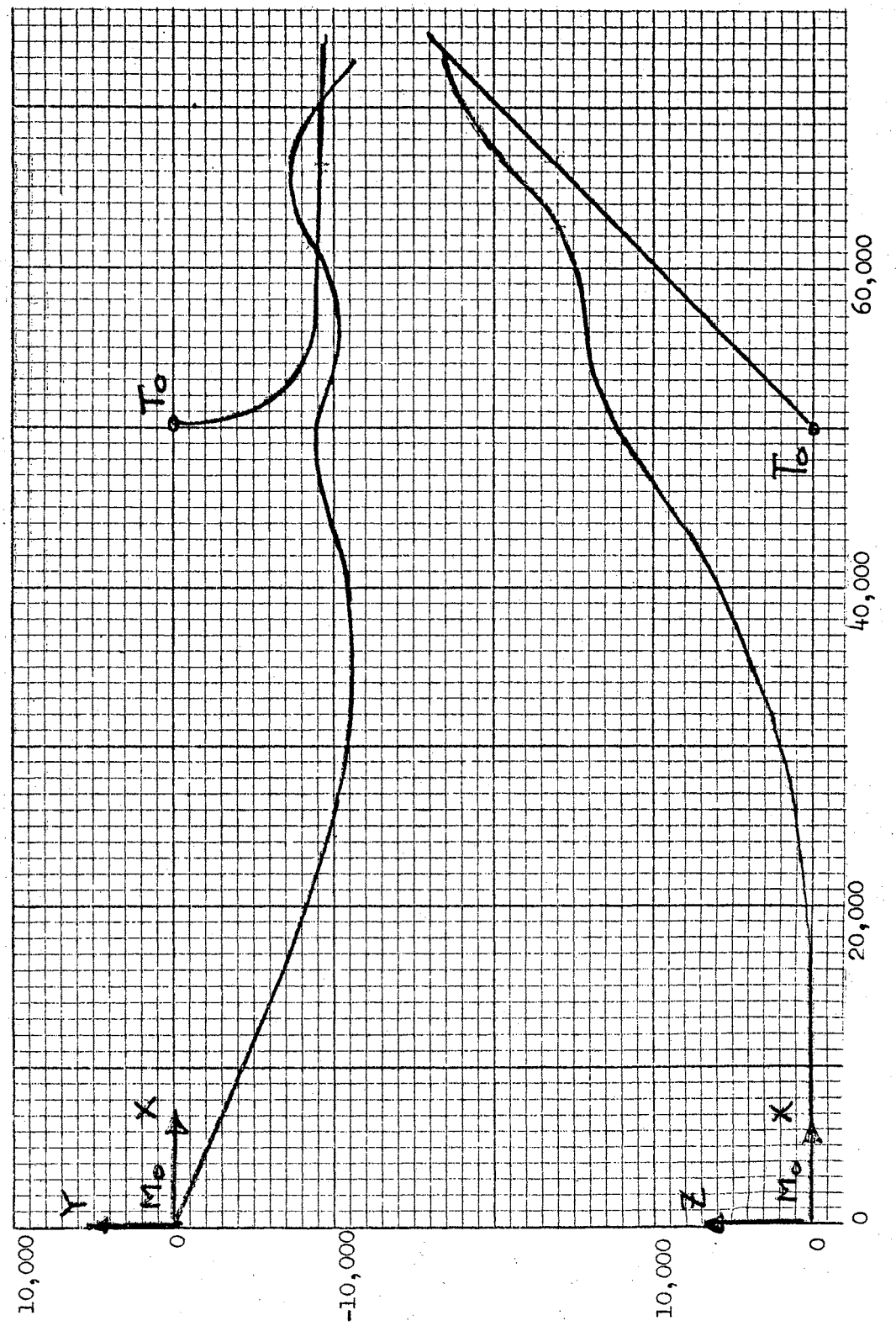

Figure 21. Encounter VI, Run 3c

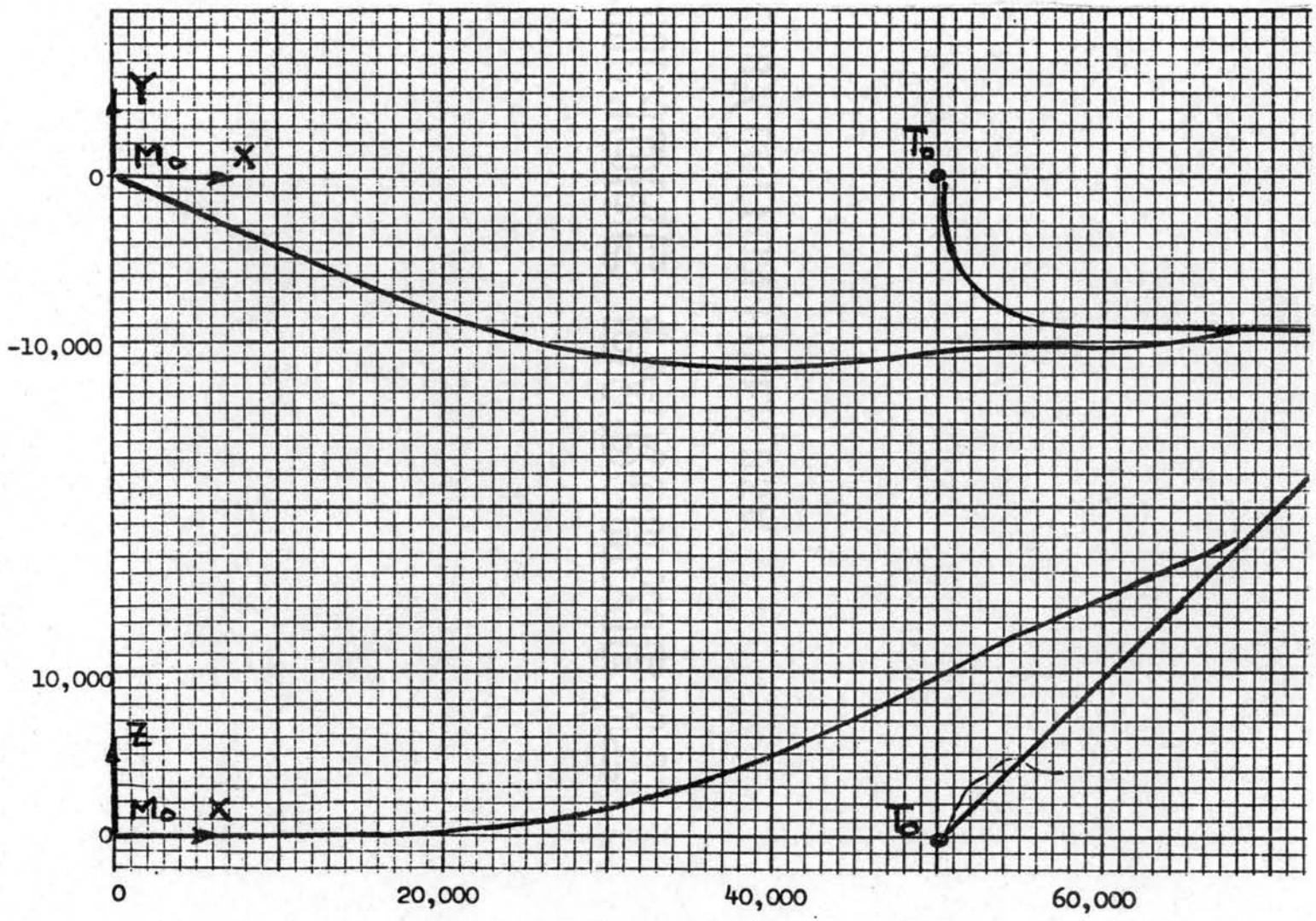

Figure 22. Encounter VI, Run 3d

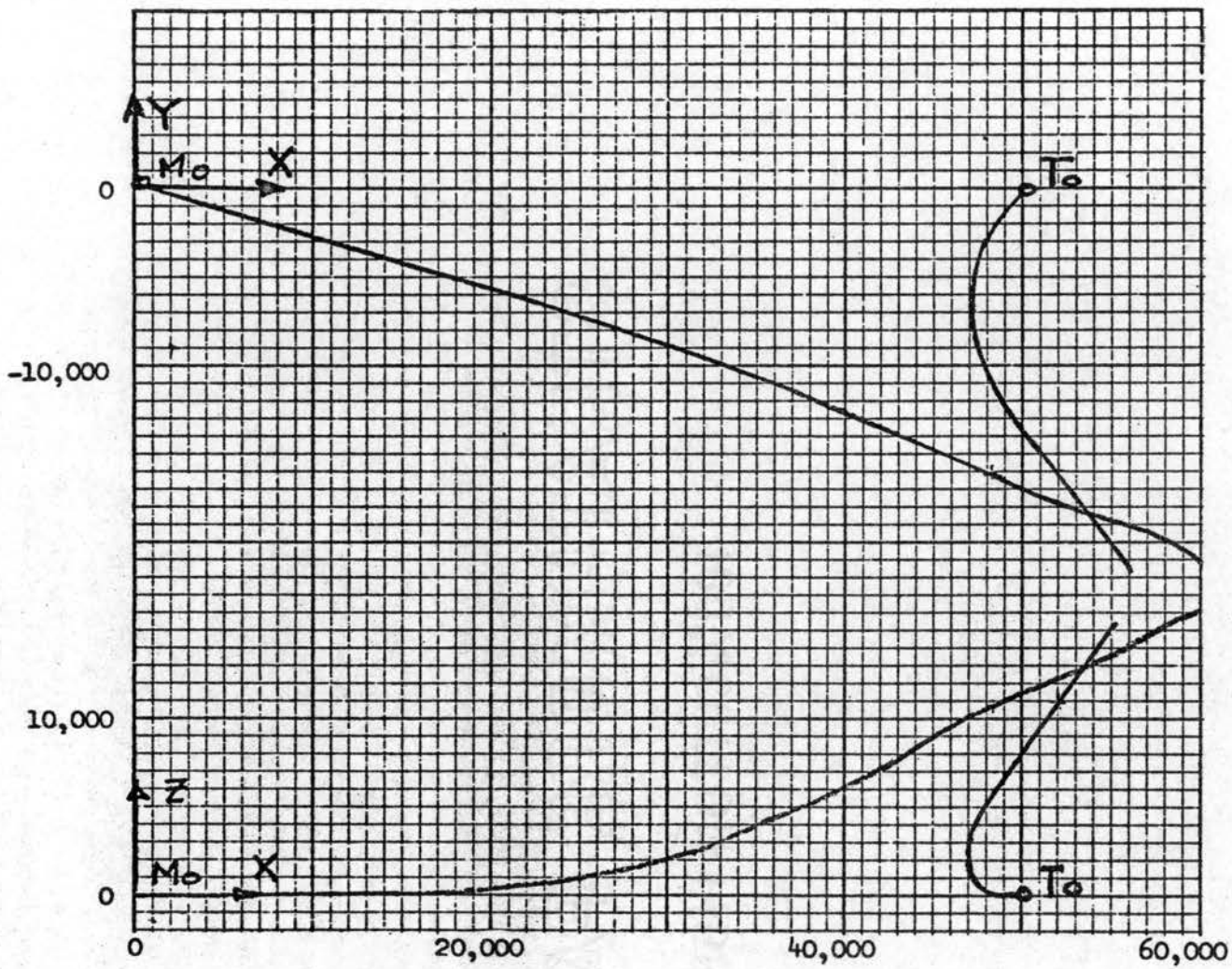

Figure 23. Encounter VI, Run 4c

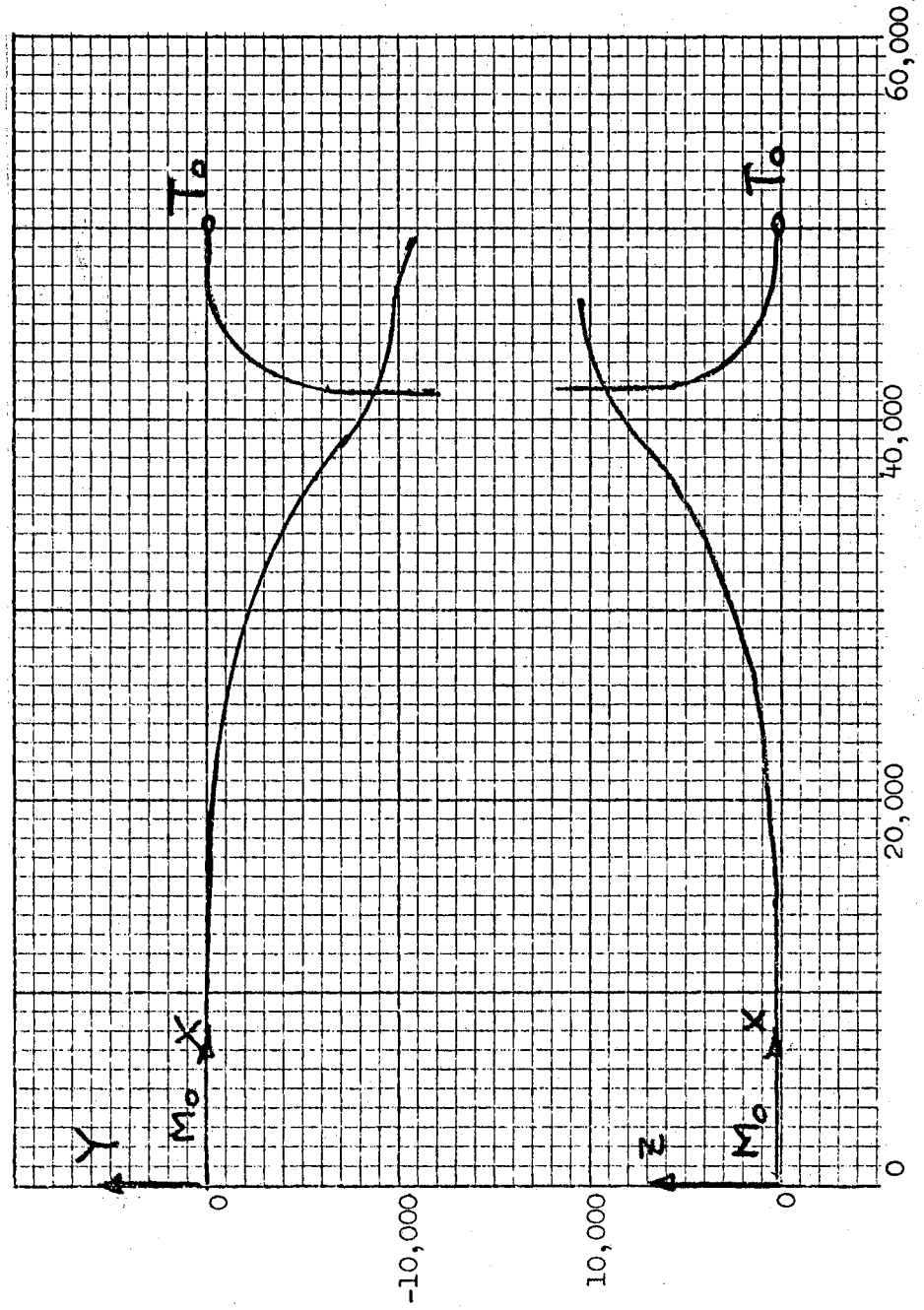

Figure 24. Encounter VI, Run 5a

TABLE VI

CALIBRATION RESULTS

Run No.	Time From Zero Sec.	Range to Target ft.	Missile Heading			Range Rate $\dot{R}$ fps.	Target Heading			Remarks
			α_x Degrees	α_y Degrees	α_z Degrees		α_x Degrees	α_y Degrees	α_z Degrees	
1	0	50,000	0	90	90	-1500	0	90	90	Collision course
1	29.6	0	-16.4	106.4	90	-1668	-45	135	90	M. H. and T. H.*
2	0	50,000	0	90	90	-1500	0	90	90	Collision course
2	29.6	0	16.4	90	73.6	-1668	45	90	45	M. H. and T. H.
3	0	50,000	0	90	90	-1500	0	90	90	Collision course
3	21.8	0	23.6	66.4	90	-2290	90	0	90	M. H. and T. H.
4	0	50,000	0	90	90	-1500	0	90	90	Collision course
4	21.8	0	-23.6	113.6	0	-2290	-90	90	180	M. H. and T. H.
5	0	50,000	0	90	90	-3500	180	90	90	Collision course
5	21.8	0	23.6	66.4	90	-2290	90	0	90	M. H. and T. H.
6	0	50,000	0	90	90	-3500	180	90	90	Collision course
6	16.1	0	-16.4	90	106.4	-3082	-135	90	225	M. H. and T. H.
7	0	50,000	0	90	90	-3500	180	90	90	Collision course
7	16.1	0	16.4	73.6	90	-3082	135	-45	90	M. H. and T. H.

*M. H. = Missile Heading Error
T. H. = Target Heading Error

TABLE VII

POSITION AND HEADING ERROR RESULTS

Run No.	Time From Zero Sec.	Range				Range Rate				Remarks
		R ft.	α_x Degrees	α_y Degrees	α_z Degrees	$\dot{R}$ fps.	α_x Degrees	α_y Degrees	α_z Degrees	
I-0	0	50,000	0	90	90	1,500	180	90	90	Collision course
2	29.5	5,020	5	96	96	1,597	174	87	87	Missile and Target Heading
3	33.8	5,005	0	88	88	1,525	170	98	98	Missile and Target Heading and Position
3	35	3,000	0	90	90	1,525	170	82	82	Missile and Target Heading and Position
6	34	5,000	0	90	90	1,556	162	103	103	Missile and Target Heading and Position
II-0	0	50,000	0	90	90	1,668	180	90	90	Collision course
2	25.5	5,015	0	95	95	1,810	161	109	87	Missile and Target Heading
3	30	5,000	0	90	90	1,815	162	106	96	Missile and Target Hdg. and Position
5	29.5	5,000	0	90	90	1,840	165	101	79	Missile Heading and Position
III-0	0	50,000	0	90	90	2,290	180	90	90	Collision course
2	19.7	5,015	2	90	82	2,250	173	90	109	Position (z direction)
3	19	5,000	0	88	90	2,300	178	93	90	Position (y direction)

TABLE VII (Continued)

Run No.	Time From Zero Sec.	Range				Range Rate				Remarks
		R ft.	α_x Degrees	α_y Degrees	α_z Degrees	$\dot{R}$ fps.	α_x Degrees	α_y Degrees	α_z Degrees	
III-11	24.5	5,300	19	74	82	2,510	150	120	92	Position and Missile and Target Heading
11	27	0	0	90	90	2,190	169	102	98	Position and Missile and Target Heading
IV-0	0	50,000	0	90	90	3,082	180	90	90	Collision course
1	14.5	5,020	5	96	96	3,000	172	84	85	Missile Heading
3	17.5	5,280	19	71	90	2,720	160	70	89	Missile and Target Headings
4	15.8	5,010	2	93	90	2,910	162	81	108	Missile Heading and Position
V-0	0	50,000	0	90	90	3,500	180	90	90	Collision course
3	11.5	5,600	26	90	64	3,100	154	74	109	Missile and Target Heading and Position
4	13.3	5,340	20	78	74	3,290	170	84	98	Pos. and Target Heading
5	11.7	5,440	28	74	74	3,460	163	102	102	Position

TABLE VIII

TARGET MANEUVER RESULTS

Run No.	Time From Zero Sec.	Range				Range Rate				Remarks
		R ft.	α_x Degrees	α_y Degrees	α_z Degrees	$\dot{R}$ fps.	α_x Degrees	α_y Degrees	α_z Degrees	
VI-1c	0	50,000	0	90	90	1,500	180	90	90	Collision course
	23	5,900	32	70	68	1,960	169	97	98	3g. maneuver
VI-2b	0	50,000	0	90	90	1,668	180	90	90	Collision course
	28.5	5,100	11	79	88	1,455	144	114	115	2g. maneuver
2c	32.5	5,480	24	111	101	1,825	162	76	77	3g. maneuver
2d	28	5,480	24	69	79	1,385	137	122	99	3g. maneuver
2d	33	0	0	90	90	2,070	155	97	97	3g. maneuver
2e	26.5	5,220	17	78	78	1,700	146	124	98	2g. maneuver
VI-3c	0	50,000	0	90	90	2,290	180	90	90	Collision course
	27.5	5,200	16	101	89	1,530	146	133	98	3g. maneuver
3d	26.5	5,200	16	12	11	1,410	175	90	96	3g. maneuver
3d	29.5	1,400	44	60	60	1,425	141	164	105	3g. maneuver
VI-4a	0	50,000	0	90	90	3,182	180	90	90	Collision course
	16	3,000	0	90	90	2,110	169	91	101	1g. maneuver
4c	21.5	3,060	10	90	83	1,470	170	90	98	3g. maneuver
VI-5a	0	50,000	0	90	90	3,500	180	90	90	Collision course
	16	4,030	6	94	96	1,920	168	84	97	3g. maneuver

CHAPTER VI

SUMMARY AND CONCLUSIONS

Summary

Development of a technique for simulation of mid-course guidance of anti-air missile systems, capable of being extended to a variety of real systems, was the main goal of this research. The technique simulates mid-course guidance in which the missile dynamics and control systems are included as sequential sub-systems. The technique includes provision for finding the range and range rate of the missile-target system as the target maneuvers in three dimensions and as various heading and position errors occur.

An introduction to the subject of anti-air missile systems and their guidance techniques was presented in Chapter I. The mid-course guidance was described as occurring after launch and prior to terminal encounter. Various guidance schemes and courses were discussed, including the proportional guidance used in this research. Proportional guidance was described mathematically by Equations (1.1) through (1.9).

In Chapter II, the unclassified historical contributions were presented. It was concluded that the techniques

described in literature pertinent to this research are mainly in two dimensions, lack versatility, and, in some cases, use questionable mathematical techniques.

Chapter III contains the extension to three dimensions of the missile-target simulation and, also, the various systems of equations which are needed in the following chapter to program the analog computer. After establishing certain necessary reference systems, the line of sight (range) vector and range rate vector were expressed in terms of their scalar components. The missile velocity was then placed in the same reference frame as the range and range rate vectors. Proportional guidance was related to the turning rates of the line of sight and missile velocity by the assumption that the missile was well designed dynamically. A linearization of the system of nonlinear differential equations was carried out using a Taylor series expansion about the collision course. The perturbed set of linear differential equations, some with time varying coefficients, was obtained. Certain nonlinear approximations were made to the linearized set of equations. These approximations later were shown to give the best results.

Chapter IV presents the analog computer simulation. The unscaled set of equations were brought forth from the preceding chapter, and were presented as Equations (4.1) through (4.26). The encounter conditions for missile and target heading errors and position errors were described

along with the target maneuver encounters. The estimated maximum value of the perturbed variables was then presented, and the scaled computer diagram drawn.

The analog computer simulation results were presented in Chapter V. The data was presented in the form of tables and figures, and discussed, wherever necessary. A series of system calibration encounters was explained in detail because they essentially show that the system of equations was correctly simulated by the analog computer.

The results of the encounters between missile and target with heading and position errors were presented and discussed. It was shown that range and range rate can be determined from the simulation for heading and position errors. Also presented in Chapter V were the results of the target maneuver. It was shown that the approximations given by Equations (3.75) through (3.78) for the line of sight turning rate gave the best results. It was further shown that of the 56 runs made, 22 were direct hits, 15 were within 500 feet of the target, and the remaining 19 could have been brought within 500 feet by repeating the experiments using the approximations stated preceding.

Conclusions

The research described herein leads to the following general conclusions:

1. Extension of the anti-air missile encounter to three dimensions yields a system of

nonlinear, ordinary differential equations in which the missile dynamics and control system appear as a sequential sub-system.

2. The simulation technique is capable of being extended to realistic missile systems by selecting the proper pitch and yaw transfer functions including the coupling between the pitch and yaw modes.
3. The simulation yields the miss distance (range at $R_x = 0$), its attitude, range or closing rate, and its attitude for heading and position errors, as well as target maneuver. These are the inputs to the terminal phase of the flight.
4. Certain system calibration encounters which were carried out verify that the analog computer was properly programmed, and that the system of approximate nonlinear equations simulated the mathematical description of the missile-to-target flight.
5. Use of the x component of range (R_x) for the rate of change of the line of sight calculation in proportional guidance is the best means of approximate simulation. This is due, mainly, to its capability of being updated in flight.
6. The experimental results give credence to the

validity of the hypothesized simulation of mid-course guidance in an anti-air missile-target encounter.

Recommended Future Studies

This research has brought to light certain promising areas of future study. These areas are:

1. Modification of the present system for more efficient use. Reprogram the system with the view of data collection rather than experimental verification. This requires reprogramming and rescaling. With more electronic equipment available, the system could be programmed for the original non-linear system.
2. The research should be repeated for statistical inputs of heading errors, sensor noise, target maneuver, and system delays.
3. A comparison between analog (continuous variable) and digital computer (discrete variable) calculation techniques should provide quantitative data of higher accuracy on miss distance. This is particularly true since the groundwork has been laid using the analog computer.
4. A hybrid computer study should utilize the

best features of both the analog and the digital computer.

A SELECTED BIBLIOGRAPHY

1. _____. Weapons Systems Fundamentals, Analysis of Weapons. Washington, D. C.: NAVWEPS, O.P. 3000, Vol. 2, 1960.

2. Dow, R. B. Fundamentals of Advanced Missiles. New York: Wiley, 1958.

3. Merrill, Grayson, ed. Principles of Guided Missile Design, Vol. 1, Guidance. Princeton, New Jersey: D. Van Nostrand, 1955.

4. Merrill, Grayson, ed. Principles of Guided Missile Design, Vol. 7, Systems Preliminary Design. Princeton, New Jersey: D. Van Nostrand, 1960.

5. Clemow, J. Missile Guidance. London, England: Temple Press, 1962.

6. Rogers, A. E., and T. W. Connolly. Analog Computation in Engineering Design. New York: McGraw-Hill, 1960, pp. 370-377.

7. Siry, J. W. "The Early History of Rocket Research." Sci. Monthly, 71, 1 (1950).

8. Goddard, R. H. Rockets. New York: American Rocket Society, 1946.

9. Goddard, R. H. Rocket Development. Englewood Cliffs, New Jersey: Prentice-Hall, 1948.

10. Dornberger, Walter. V-2. New York: Viking Press, 1954.

11. Newell, H. E., Jr. Nav. Res. Lab Rept. R-2538. May 22, 1945.

12. Adler, Fred P. "Missile Guidance by Three Dimensional Proportional Navigation." Journal of Applied Physics, Vol. 27, No. 5 (May, 1956).

13. Yuan, L. C. "Homing and Navigational Courses of Automatic Target-Seeking Devices." Journal of Applied Physics, Vol. 19 (Dec., 1948).

14. Burt, E. G. C. "Theoretical Principles of Guided Missile Systems." Journal of the Royal Aero. Soc., Vol. 63 (Aug., 1959).

15. Waymeyer, W. K., and T. H. Young. "Coupling in Cruciform-Missile Control Systems." I.E.E.E. Trans. Appl. and Ind., V. 83, n. 75 (Nov., 1964).

16. Waymeyer, W. K., and R. W. Sporing. "Closed Loop Adaptation Applied to Missile Control." J.A.C.C. Paper 18-3, 1962.

17. Halfman, R. L. Dynamics. Vol. I. Reading, Mass.: Addison-Wesley, 1962.

18. Meriam, J. L. Dynamics. New York: John Wiley and Sons, 1966.

19. Nelson, W. C., and E. E. Loft. Space Mechanics. Englewood Cliffs, New Jersey: Prentice-Hall, 1962.

20. D'Azzo, J. J., and C. H. Houpis. Feedback Control System Analysis and Synthesis. New York: McGraw-Hill, 1966, Chapter 8.

21. Kuo, B. C. Automatic Control Systems. Englewood Cliffs, New Jersey: Prentice-Hall, 1964, Chapter 5.

APPENDIX A

AXIS TRANSFORMATIONS

In the course of this study, it was necessary to transform from cartesian (i.e., rectangular) coordinates to cylindrical or to spherical coordinates. This appendix presents the particular notation used and can be found in Halfman (17), Meriam (18), or Nelson and Loft (19).

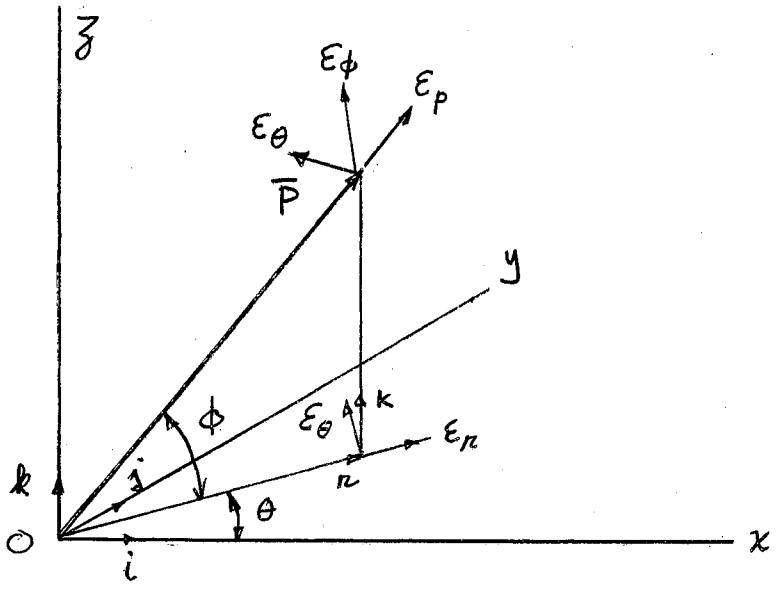

Figure 25. Coordinate Systems

The vector $\bar{P}$ may be written in the three different coordinate systems as follows:

$$\bar{P}(x,y,z) = P_x i + P_y j + P_z k, \qquad (AA.1)$$

$$\bar{P}(r,\theta,z) = P_r \varepsilon_r + P_\theta \varepsilon_\theta + P_z k \qquad (AA.2)$$

or

$$\bar{P}(P,\theta,\varphi) = P_p \varepsilon_p + P_\theta \varepsilon_\theta + P_\varphi \varepsilon_\varphi \ . \qquad (AA.3)$$

These are all the same P, only with different directions of resolution. To express the components of one set of directions in terms of the components in another set of directions is a useful and necessary part of this study. There are six possible transformations which will be shown.

Rectangular-Cylindrical

To transform from rectangular coordinates to cylindrical coordinates

$$\begin{bmatrix} P_r \\ P_\theta \\ P_z \end{bmatrix} = \begin{bmatrix} \text{Cos}\,\theta & \text{Sin}\,\theta & 0 \\ -\text{Sin}\,\theta & \text{Cos}\,\theta & 0 \\ 0 & 0 & 1 \end{bmatrix} \begin{bmatrix} P_x \\ P_y \\ P_z \end{bmatrix} \qquad (AA.4)$$

is used. Equation (AA.4) is also valid for a rotation of θ about the z axis. The inverse transformation is

$$\begin{bmatrix} P_x \\ P_y \\ P_z \end{bmatrix} = \begin{bmatrix} \text{Cos}\,\theta & -\text{Sin}\,\theta & 0 \\ \text{Sin}\,\theta & \text{Cos}\,\theta & 0 \\ 0 & 0 & 1 \end{bmatrix} \begin{bmatrix} P_r \\ P_\theta \\ P_z \end{bmatrix} , \qquad (AA.5)$$

which also is a rotation about the z axis, but by a negative θ.

Cylindrical-Spherical

To transform from cylindrical to spherical coordinates the expression

$$\begin{bmatrix} P_p \\ P_\theta \\ P_\varphi \end{bmatrix} = \begin{bmatrix} \text{Cos}\,\varphi & 0 & \text{Sin}\,\varphi \\ 0 & 1 & 0 \\ -\text{Sin}\,\varphi & 0 & \text{Cos}\,\varphi \end{bmatrix} \begin{bmatrix} P_r \\ P_\theta \\ P_z \end{bmatrix} \qquad \text{(AA.5)}$$

is used. The inverse from spherical to cylindrical coordinates is

$$\begin{bmatrix} P_r \\ P_\theta \\ P_z \end{bmatrix} = \begin{bmatrix} \text{Cos}\,\varphi & 0 & -\text{Sin}\,\varphi \\ 0 & 1 & 0 \\ \text{Sin}\,\varphi & 0 & \text{Cos}\,\varphi \end{bmatrix} \begin{bmatrix} P_p \\ P_\theta \\ P\varphi \end{bmatrix} . \qquad \text{(AA.6)}$$

Rectangular-Spherical

To transform from rectangular to spherical coordinate, the expression is

$$\begin{bmatrix} P_p \\ P_\theta \\ P_\varphi \end{bmatrix} = \begin{bmatrix} \text{Cos}\,\varphi\ \text{Cos}\,\theta & \text{Cos}\,\varphi\ \text{Sin}\,\theta & \text{Sin}\,\varphi \\ -\ \text{Sin}\,\theta & \text{Cos}\,\theta & 0 \\ -\text{Sin}\,\varphi\ \text{Cos}\,\theta & -\text{Sin}\,\varphi\ \text{Sin}\,\theta & \text{Cos}\,\varphi \end{bmatrix} \begin{bmatrix} P_x \\ P_y \\ P_z \end{bmatrix} . \qquad \text{(AA.7)}$$

Its inverse is

$$\begin{bmatrix} P_x \\ P_y \\ P_z \end{bmatrix} = \begin{bmatrix} \text{Cos}\,\varphi\ \text{Cos}\,\theta & -\text{Sin}\,\theta & -\text{Sin}\,\varphi\ \text{Cos}\,\theta \\ \text{Cos}\,\varphi\ \text{Sin}\,\theta & \text{Cos}\,\theta & -\text{Sin}\,\varphi\ \text{Sin}\,\theta \\ \text{Sin}\,\varphi & 0 & \text{Cos}\,\varphi \end{bmatrix} \begin{bmatrix} P_p \\ P \\ P_\theta \end{bmatrix}. \tag{AA.8}$$

The transformations (AA.4) to (AA.8) hold for any vector. An additional relationship is the time derivative of the P vector which is

$$\dot{\bar{P}} = \dot{P}\varepsilon_p + P\,\dot{\theta}\ \text{Cos}\,\varphi\ \varepsilon_\theta + P\dot{\varphi}\varepsilon_\varphi \tag{AA.9}$$

in spherical coordinates and

$$\dot{\bar{P}} = \dot{P}_x i + \dot{P}_y j + \dot{P}_z k \tag{AA.10}$$

in rectangular coordinates. It is further noted that

$$\dot{\varepsilon}_p = \dot{\theta}\ \text{Cos}\ \varphi\varepsilon_\theta + \dot{\varphi}\varepsilon_\varphi\,. \tag{AA.11}$$

APPENDIX B

POTENTIOMETER AND AMPLIFIER ASSIGNMENTS

Potentiometer		Amplifier	
No.	Parameter	No.	Output Variable
00	0.05 Cos L	01	$10^{-5}\ \rho_{MX}$
01	0.02 Sin A	02	$2 \times 10^{-5}\ \rho_{tY}$
02	0.05 Sin L	03	$2 \times 10^{-5}\ \rho_{MY}$
03	0.02 Cos A	04	0.5λ
04	$2 \times 10^{-5}\ \rho_{tYo}$	05	-0.5γ
05	$10^{-5}\ R_{Y}po$	07	5γ
06	$K\ \omega_n^2$	08	0.5γ
07	0.025 Cos L	09	time
08	ω_n^2	10	$5\mathring{\sigma}$
09	0.02 Sin A	11	-0.5σ
10	0.1	12	$10^{-4}\ \rho_{MZ}$
11	$K\ \omega_n^2$	13	$10^{-4}\ \rho_{tZ}$
12	ω_n^2	14	$2 \times 10^{-5}\ R_X$
13	$2\zeta\omega_n$	15	$2 \times 10^{-5}\ R_Y$
15	$2 \times 10^{-5}\ \rho_{tXo}$	16	$-2 \times 10^{-5}\ \rho_{tY}$
18	0.025 Sin L	17	$10^{-5}[\lambda][\mathring{R}_1 t]$
20	0.2	20	-5×10^{-4} at
21	0.5	21	$-4 \times 10^{-4}\mathring{y}$
22	0.05 Sin L	22	$10^{-3}\mathring{u}$

Potentiometer		Amplifier	
No.	Parameter	No.	Output Variable
23	$2\zeta\omega_n$	23	0.5σ
24	$10^{-4}\rho_{tzo}$	24	$10^{-4}R_z$
25	0.2	25	$-10^{-5}[\rho_{tx} + R_o]$
26	0.2	26	-0.5δ
27	0.02 Cos A	28	$4 \times 10^{-4}\dot{x}$
28	0.02 Cos A	29	$2 \times 10^{-5}\ \dot{R}_1 t$
29	$4 \times 10^{-4}\dot{y}_o$	30	5×10^{-4} at
30	0.05(Cos L - 0.4 Cos A)	31	$4 \times 10^{-4}\dot{z}$
31	0.25 Cos L	33	$1 + (4 \times 10^{-4}\dot{x})^2$
32	0.02 Sin A	34	-A33
33	0.25	36	$-2 \times 10^{-5}\dot{R}_1 t$
34	0.1	37	$2 \times 10^{-5}\ \rho_{tx}$
35	$10^{-5}R_{zpo}$	38	$-10^{-4}\ \rho_{tx}$
36	0.1	42	$-4 \times 10^{-4}\ \dot{x}$
39	$4 \times 10^{-4}\ \dot{z}_o$	43	$4 \times 10^{-4}\ \dot{z}$
40	0.02	44	$4 \times 10^{-4}\ \dot{y}$
43	0.2	66	0.5λ
45	0.1	67	0.5δ
48	$10^{-5}\ R_{ypo}$	68	$-10^{-5}\ \delta\ \dot{R}_1 t$
49	$10^{-5}\ R_{zpo}$	69	$-10^{-3}\ \dot{u}$
53	0.5	70	$-1.6 \times 10^{-7}\ \dot{z}^2$
54	0.5	71	$10^{-5}(\rho_{tx} + R_o)$
55	0.01 n	72	$-1.6 \times 10^{-7}\ \dot{y}^2$
56	0.2		
58	0.1		

VITA

Edwin James Waller

Candidate for the Degree of

Doctor of Philosophy

Thesis: MID-COURSE GUIDANCE SIMULATION FOR ANTI-AIR MISSILE SYSTEMS

Major Field: General Engineering

Biographical:

Personal Data: Born near Claremore, Oklahoma, July 16, 1925, the son of William R. and Nelle Waller.

Education: Attended grade schools at Claremore and Tiawah, Oklahoma, at Winfield and Herrington, Kansas; attended secondary schools at Tahlequah, Alluwe, and Enid, Oklahoma; attended Oklahoma State University, Stanford University, and Maryland University; received Degrees of Bachelor of Science (1949) and Master of Science (1951), both in General Engineering, at Oklahoma State University; received the Degree of Engineer from Stanford University, with a major in Engineering Mechanics, in 1959; completed requirements for the Doctor of Philosophy Degree in November, 1967.

Professional Experience: Entered the United States Army in February, 1942 and was honorably discharged in October, 1945; was employed by the Division of Engineering Research, Oklahoma State University, upon graduation in 1951; served as an Instructor, later Assistant Professor in the School of Civil Engineering, Oklahoma State University from June, 1951 until September, 1955, and as Associate Professor from October, 1956 until July, 1964; was a Research Engineer, Carter Oil Research Laboratory, Tulsa, Oklahoma, from September, 1955 until October, 1956; was

appointed Associate Professor of Weapons, United States Naval Academy, Annapolis, Maryland, in July, 1964, an appointment presently held; received two Science Faculty Fellowships from the National Science Foundation, the first from June, 1958 through September, 1959, and the second from January, 1967 through January, 1968; has been active as a consultant in the fields of dynamics, fluid flow, and pressure surges in pipelines, from 1954 to the present.

Professional Organizations: A Registered Professional Engineer in Oklahoma; Member of the American Society of Engineering Education; Member of the American Society of Mechanical Engineers; Member of Sigma Xi and Phi Kappa Phi.